ISSN: 1648-6897 / eISSN: 1822-4199

VILNIUS TECH
Vilnius Gediminas Technical University

JOURNAL of ENVIRONMENTAL ENGINEERING & LANDSCAPE MANAGEMENT

2026
Volume 34
Issue 2
Pages 235–254
https://doi.org/10.3846/jeelm.2026.27720

ACTIVATED CARBON LOADED WITH Fe@Fe_2O_3 AND CeO_2 AS A NOVEL COMPOSITE CATALYST FOR HETEROGENEOUS ELECTRO-FENTON PROCESS

Asyah R. FLAYYIH[1]✉, Wadood T. MOHAMMED[1], Ali H. ABBAR[2]

[1]*Department of Chemical Engineering, College of Engineering, University of Baghdad, 10071 Baghdad, Iraq*
[2]*Department of Biochemical Engineering, Al-Khwarizmi College of Engineering, University of Baghdad, 10071 Baghdad, Iraq*

Highlights:

- a novel composite heterogeneous electro-Fenton (HEF) catalyst was successfully prepared;
- AC+Fe/Ce (2:1) is the best HEF catalyst which gave higher methylene blue removal (91%);
- AC+Fe/Ce (2:1) as HEF catalyst also gave higher COD removal (83.4%);
- HEF system has the ability to operate at neutral condition with good removal of COD (78.83%);
- current density is the main operating variable governing the electrochemical reactions in the process.

Article History:

- received 23 August 2025
- accepted 03 November 2025

Abstract. A novel heterogeneous electro-Fenton (HEF) composite catalyst based on activated carbon (AC) as the support material was prepared with the inclusion of Fe@Fe_2O_3 for its HEF catalytic activity and cerium oxide (CeO_2) for its redox properties. The effect of different Fe/Ce molar ratios on the activity of the prepared catalysts was investigated. XRD, BET, FTIR, SEM, and EDS techniques were used to characterize the prepared catalysts. The catalyst activity was examined by its ability to degrade 50 mg/L of methylene blue (MB) at 20 mA/cm^2 and pH 3 within 150 min. A higher removal rate of 91% was achieved when AC+Fe/Ce (2:1) was used as a HEF catalyst. The results confirmed the synergy between Fe and Ce at a Fe/Ce molar ratio of 2:1. This improved catalyst was used to remove chemical oxygen demand (COD) from petroleum refinery wastewater. The optimum conditions were a current density of 10 mA/cm^2, pH of 3, and a catalyst dosage of 1 g/L, achieving a COD removal rate of 83.4%, with an energy consumption of 9.22 kWh/kg COD. Reusability testing confirmed the good catalytic activity of AC+Fe/Ce (2:1) catalyst after five cycles. Furthermore, the COD degradation over time was found to follow pseudo-first-order kinetics. These findings demonstrate that the prepared AC+Fe/Ce (2:1) catalyst is a highly efficient and energy-effective material for degrading organic pollutants in wastewater.

Keywords: Fe@Fe_2O_3, cerium oxide, petroleum refinery, heterogeneous catalysts, carbon supported materials.

✉Corresponding author. E-mail: *asiyah.falih2207@coeng.uobagdad.edu.iq*

1. Introduction

Organic pollutants pose a problem with the rise in population, industrialization, and urbanization (Soufi et al., 2021). This growth in human activities leads to the interaction of refractory organic pollutants in various industrial applications such as textile and petroleum industries. These pollutants can remain in the ecosystem for a long time, increasing the risk of cariogenic effect on living organisms (Li et al., 2021). To reduce the hazardous effect of these refractory organic compounds, various methods have been used, including membrane separation, adsorption, biological treatment, and advanced oxidation processes (AOPs) (Sadek et al., 2025; Liu et al., 2025; Atiyah et al., 2024; Jiad & Abbar, 2023a, 2023b; Thorat & Sonwani, 2022; Sathya et al., 2022). Among these techniques, AOPs have been widely used over the past two decades due to their efficiency in generating strong reactive oxygen species during treatments (Kumari & Kumar, 2023; Pournamdari et al., 2024; Deylami et al., 2023).

Fenton process is a powerful method within AOPs used to treat various organic pollutants from textile and petroleum industry effluents (Hilsendeger et al., 2025; Patil & Raut, 2014; Elmobarak et al., 2021). It is a cost-effective and robust method that generates HO$^\bullet$ via the reaction between H_2O_2 and Fe^{2+} in acidic media (pH ≈ 3) (Mirzaei et al., 2017). However, the classic homogeneous Fenton has several disadvantages such as the need to provide a large amount of H_2O_2 that must be handled and stored, limited catalyst regeneration, waste sludge generation, instability of H_2O_2, and narrow pH range (2.8-3) during the operation (Jiad & Abbar, 2023b; Mohammadi et al., 2024).

Therefore, a modification of this process was proposed by combining Fenton with an electric current in a process known as homogenous electro-Fenton (EF). In this process, not only hydrolysis of water on the anode is happened, thus generating more radicals, but also enables the generation of hydrogen peroxide (H_2O_2) on the cathode by reducing oxygen (O_2) supplied externally in the form of air. Furthermore, regeneration of Fe^{2+} occurs by reducing Fe^{3+} on the cathode, hence decreasing iron sludge formation (Fan et al., 2023; Fahim & Abbar, 2020). Additionally, EF is a cost effective method in comparison with AOPs. It exhibits a treatment cost in the range from 0.5 to 2.5 USD/m^3 while photocaltytic method needs for a treatment cost in the range from 1.5 to 4 USD/m^3 as well as ozonation in the range from 2 to 6 USD/m^3 (Brillas & Martínez-Huitle, 2015).

However, homogenous EF still suffers from limited pH application rang, generation of iron sludge, and non-reusable catalyst (Zhu et al., 2019). To overcome these issues, HEF process was developed where catalyst modification was the most important research tasks (Fan et al., 2023; Jinisha et al., 2018; Yang et al., 2020). In this field, several HEF catalysts have been used to activate hydrogen peroxide to generate $HO^{\bullet}$ including pyterite (Ye et al., 2020), Fe-based bimetallic catalyst (Luo et al., 2020), chalcopyrite (Barhoumi et al., 2017), and α-FeOOOH (Sánchez-Sánchez et al., 2007). However, these catalysts suffer from excessive agglomeration and dissolution of iron elements, resulting in a large amount of sludge. Therefore, developing an effective and stable iron-based HEF catalyst remains a challenge.

Recently, zero-valent iron catalysts have been used as an efficient and environmentally friendly HEF catalyst which can act bifunctionally, as adsorbent and catalyst during the HEF process (Zhang et al., 2020; GilPavas & Correa-Sanchez, 2019; Guo et al., 2023). They are low cost, having strong reducing ability and good catalytic activity (Nidheesh & Gandhimathi, 2014). However, zero valent iron catalyst are highly reactive, making them difficult to handle or store, as well as having a tendency to aggregate with passivation (Chen et al., 2019). Therefore, zero valent iron has been supported on materials such as zeolite, bentonite, activated carbon (AC), charcoal, and others to inhibit the aggregation (Azizi & Davarnejad, 2023; Tesnim et al., 2024b; Xiao et al., 2014; Wang et al., 2018; Lu et al., 2024). Among them, activated carbon has been extensively utilized due to its stable structure, high specific surface area, resistance to bases and acids, ease of recycling, and cost-effectiveness (Tesnim et al., 2024b; Thomas et al., 2021).

In the present work, a new HEF catalyst was developed by incorporating $Fe@Fe_2O_3$ and CeO_2 on an activated carbon, creating a unique composite with improved catalytic and redox properties. $Fe@Fe_2O_3$ is a type of zero-valent iron catalyst prepared by reducing iron ions with $NaBH_4$ (Amin et al., 2019; Zare et al., 2024). It was more suitable for practical applications than zero-valent iron due to several features, including accelerated electron transfer rate, high surface area, and the existing Fe_2O_3 shell, which prevents spontaneous oxidation by air and enables its transport and storage (Ai et al., 2013). Furthermore, this type of nanoparticles exhibits unique performance in EF by producing superoxide radicals by activating one and two electrons of molecular oxygen, thereby accelerating the Fe^{3+}/Fe^{2+} conversion cycle. Therefore, the generation rate of $HO^{\bullet}$ will increase up to 3 times (Azizi & Davarnejad, 2023). CeO_2 has been found to play an important role in the catalytic field. It contains a large amount of oxygen vacancy defects, due to the redox conversion between Ce^{3+} and Ce^{4+}, which is conductive to the storage and release of oxygen and thus the generation of more H_2O_2. Furthermore, Ce^{3+} has the ability to activate H_2O_2 but to a lesser extent than Fe^{2+} to generate $HO^{\bullet}$ (Xu & Wang, 2012). Therefore incorporating $Fe@Fe_2O_3$ and CeO_2 on AC could be resulted in new findings for enhancing HEF systems. No previous works have been conducted in which AC loaded with $Fe@Fe_2O_3$ and CeO_2 was used. In spite of using $Fe@Fe_2O_3$ alone without supporting material in several works for treating some organic compounds such as ciprofloxacin (Zare et al., 2024).

The effect of molar ratio of Fe/Ce loaded on a fixed amount of AC was studied. The efficiency of the prepared catalyst as HEF catalyst was also investigated, based on degrading MB as a model pollutant. The application of best prepared catalyst to remove COD from a petroleum refinery wastewater (PRW) was also investigated, enhancing the novelty of the present work, as no similar applications have been studied before.

2. Materials and methods

2.1. Chemicals and reagents

Activated carbon (AC) was purchased from Zhengzhou Kelin Company, China. It has the following specification: total surface are 950–1200 m^2/g, apparent density 460±40 kg/m^3, ash content of 5%, moisture content of 8%. Methylene blue (MB, ≥97%) was purchased from BDH Chemicals Ltd., UK. Sodium borohydride ($NaBH_4$, ≥99%) was purchased from Fluka-Garantie, Switzerland. $FeCl_3.6H_2O$ with a purity of 97% was purchased from Loba Chemie PVT Ltd, India. $Ce(NO_3)_3.6H_2O$ with a purity of 98% was purchased from Himedia Laboratories Pvt.LTD, India.

Tert-butyl alcohol (TBA, >99%) and Ethyl alcohol (EtOH, >99%) were obtained from laboratory reagent, India. p-benzoquinone (p-BQ ≥ 98%, powder) was obtained from BDH Chemicals Ltd., UK. Acetone, ethanol, Na_2SO_4, HCl, and NaOH were analytical grade purchased from Merck, Germany, and used without needing for further purification. All runs were performed using distilled water with a conductivity of 0.05 μS/cm.

2.2. Synthesis of AC loaded Fe/Ce

First, 100 g of AC was sieved, and the cut of 40 to 60 mesh was isolated and considered in preparing the catalyst. The isolated amount (75 g) was soaked in 500 mL of 5% HCl

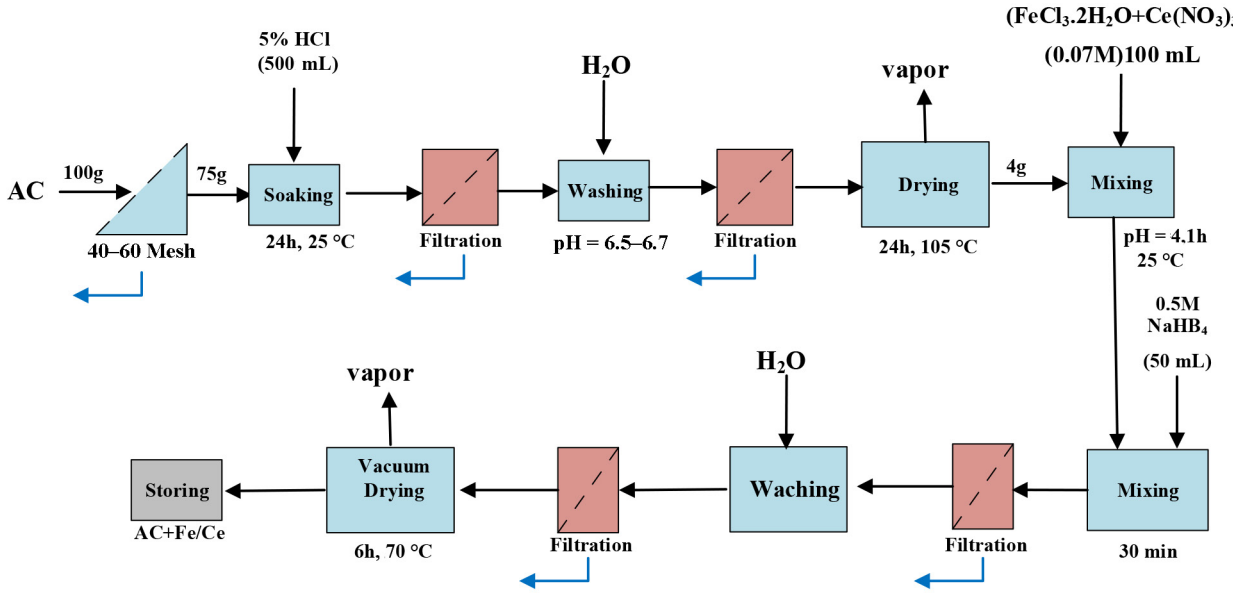

Figure 1. The schematic diagram for preparing AC+(Fe/Ce) (2:1) catalyst

for 24 h, washed with distilled solution, filtered, followed by measuring the pH of filtrate. This cycle was repeated several times until the pH of solution reached 6.5–6.7. The washed AC was dried at 105 °C for 24 h and stored until used as a supporting material. Fe@Fe_2O_3 and CeO_2 were loaded onto AC using a procedure similar to that reported in previous studies with some modifications (Azizi & Davarnejad, 2023; Xiao et al., 2014; Majlesi & Hashempour, 2017; Yazdanbakhsh et al., 2018). Briefly, for preparing a catalyst with a molar ratio (1:1) for Fe/Ce, 1.5 g $FeCl_3.6H_2O$ and 1.9 g $Ce(NO_3)_3.6H_2O$ were dissolved in 100 mL of a 30/70, v/v, ethanol-water mixture at pH 4. The prepared solution had a total concentration of 0.07 M for each salt when used separately. Maintaining the same total concentration (0.07 M) to prepare solutions containing different molar ratios of Fe/Ce from these salts. 4 g of AC was added to the above solution, and the resulting solution was mixed for 60 min at room temperature and 500 rpm. 50 mL of 0.5 M $NaHB_4$ was prepared and added dropwise (2 mL/min) to the AC-containing solution for a period of 30 min, mixing for another 30 min. The resulting catalyst was filtered, washed with ethanol and distilled water three times each, and dried in a vacuum oven at 70 °C for 6 h. The preparation method is simple and does not require air protection (Zhang et al., 2022). Hence, catalysts composed of AC loaded with either Fe or Ce alone, or with a mixture of Fe/Ce at different ratios (1:1, 2:1, 4:1) were prepared according to above procedure. The selection of 0.07 M as a total concentration of salts in preparing the catalyst is based on previous works (Xiao et al., 2014; Majlesi & Hashempour, 2017; Yazdanbakhsh et al., 2018), while selection molar ratios is based on a survey regarding to doping range of these metals on AC in previous studies with choosing the present range as a new strategy. Figure 1 shows a schematic diagram for the procedure in preparing AC+(Fe/Ce) (2:1) catalyst.

2.3. Characterization of AC loaded with Fe and/or Ce

The morphology of each catalyst was examined using scanning electron microscopy (SEM) device, Czech Republic. It was operated at HV = 25 kV, spot = 8.0, and bias = 1400 V. The crystalline structure of each catalyst was identified using X-ray diffraction (XRD) device, Panalytical X`pert Pro, Netherlands. It was operated at 40 kV, 30 mA, step size of 0.2°, and scan step time of 1.2 s. The testing was performed in the range of 2θ between 20 and 80°. FTIR measurement for each catalyst was performed using Bruker Tensor 27 device, Germany. It was operated at range 4000–400 cm^{-1} with a resolution of 1 cm^{-1} and employing KBr pellets. The specific surface area (BET) for each catalyst was measured using surface area analyzer, Thermo Company, USA. To determine the point of zero charge (pHpzc), 0.1 g of AC alone or loaded with Fe/Ce was placed in 50 mL (0.01 mol/L) at pH values between 2 and 10 and stirred for 24 h at room temperature (Atiyah et al., 2024). After that, pHpzc was determined by plotting the change in pH versus the initial value.

2.4. HEF system

The HEF system consists of: 1) electrochemical cell, 2) power supply (UNI-T, UTP3315TFL-II, China), 3) overhead stirrer (Heidolph overhead stirrer company, Germany), 4) air pump (HAILEA, Aco-318, China), 5) Ammeter (UNI-UT39C+, China), and air flow meter (Flowtech-z-7002, China). Figure 2 displays the schematic diagram of HEF system.

The HEF system is based on an electrochemical cell with a novel design. It consists of a cell body and its cover: a microporous air diffusion cathode, and a porous graphite anode.

The cell body is a cylindrical Perspex vessel (outer diameter = 80 mm, inner diameter = 90 mm, length =

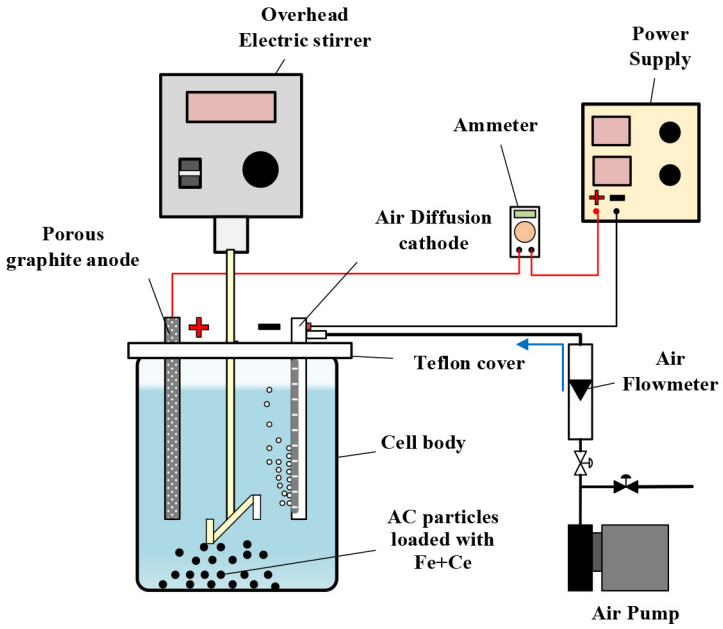

Figure 2. Schematic of the HEF system

160 mm), while its cover is a disc made of the same material, consisting of two sections: the upper (outer diameter = 120 mm, thickness = 10 mm), and the lower (outer diameter = 79 mm, thickness = 5 mm) enclosed inside the cell body. Three silts were machined on the cover: a central silt (length = 40 mm, width = 20 mm) and two other silts for inserting the cathode (length = 40 mm, width = 15 mm) and anode (length = 40 mm, width = 5 mm). The gap between the anode and cathode was fixed at 25 mm. The anode is a porous graphite plate (length = 150 mm, width = 40 mm, thickness = 4 mm) with two holes (diameter = 5 mm) located at 25 mm from the top to their centers. These holes are used to hold the anode on the cover, and make an electrical connection by two copper screws and nuts. The air-diffused cathode consists of two parts: a graphite plate and a Perspex brood cavity. The graphite plate (length = 139 mm, width = 29 mm, thickness 4 mm) was machined with 300 μm holes with a total of 60 holes, which are evenly distributed at the lower section of graphite plate (length = 60 mm, width = 30 mm). Two 4 mm diameter holes were made on the graphite plate, used to secure the plate over the brood cavity. The rectangular brood cavity (length = 150 mm, width = 40 mm, thickness 15 mm) has two cavities: an inner cavity (length = 120 mm, width = 25 mm, depth = 3 mm) and an outer cavity (length = 140 mm, width = 30 mm, depth =5 mm) for securing the microporous graphite. At the rear of the brood cavity, a 10 mm diameter hole was made for air intake, located at the center with a distance of 20 mm from the top of the brood cavity. Micropourous graphite air diffusion cathode has been proved by our previous work to have good H_2O_2 generation rate, low cost, and easy to scale-up (Jiad & Abbar, 2023b).

2.5. Activity performance

The degradation ability of prepared catalysts was determined by decolorization of MB using the HEF system described in Section 2.4. 600 mL of 50 mg/L MB solution was used, and 0.1 M sodium sulfate (Na_2SO_4) was added as a supporting electrolyte. The pH was adjusted to 3, then 0.3 g of catalyst was added to the solution to make a catalyst dosage of 0.5 g/L followed by mixing the solution for 15 min at 500 rpm. The entire solution was transferred to the electrolytic cell, and the gas diffusion cathode was supplied with air at a flow rate of 1 L/min for 15 min, followed by applying current at a current density of 20 mA/cm^2 to initiate the oxidation process. Electrolysis was performed for 150 min at room temperature, during which a sample of MB was taken and its concentration was identified by measuring the absorbance of MB at a wavelength of 665 nm using a UV-vis spectrometer (Shimadzu/Japan UV-Vis spectrometer). In investigating the catalyst activity, the pH of the solution was taken 3 below the zero charge point of iron-loaded AC. The reason is to make oxidation by hydroxyl radicals as dominant mechanism. Most of previous works reported that pH of 3 is the most suitable for degrading MB by HEF with AC loaded with iron (Lu et al., 2024; Compton et al., 2023; Sun et al., 2024; Fayazi & Ghanei-Motlagh, 2020).

2.6. Characterization and treatment of PRW

The performance of the AC catalyst loaded with Fe/Ce (2:1) in removal of COD from PRW was evaluated using the same HEF described in Section 2.4. PRW was taken from Al-Dora refinery plant located at Baghdad province-Iraq. The characteristics of wastewater are listed in Table 1.

Table 1. Characteristics of PRW

Characteristic	pH	TDS	Phenol	COD	BOD	Oil	Cl^-	Turbidity
Value	6.6	1366 mg/L	18.5 mg/L	307 mg/L	140 mg/L	20.2 mg/L	840 mg/L	35 NTU

Briefly, 600 mL of wastewater was used and Na_2SO_4 was added as a supporting electrolyte with concentration of 0.1 M. The pH of the resulting solution was adjusted to the desired value. Then, 0.6 g of catalyst was added to make a catalyst dosage of 1 g/L. the solution was mixed for 15 min. The entire solution was then transferred to the electrolytic cell and the required current was applied at a certain current density. The electrolysis continued for 90 min, during which samples of the solution were taken to determine their COD values. COD was determined using photometer (Type-MD 200 COD VARIO Photometer, Lovibond, Germany) after digesting the sample with dichromate at 150 ^{0}C for 120 min using thermo reactor type (RD-125, Lovibond).

The COD removal efficiency (*RE*%) was evaluated by Eq. (1) (Ghjair & Abbar, 2023):

$$RE\% = \frac{C_o - C_f}{C_o} \times 100, \quad (1)$$

where C_f and C_o denotes the final and initial values of COD (mg/l). The same equation was used in determine *RE* % for MB removal but in terms of MB concentrations in mg/L.

The specific energy consumption (SEC) is the energy consumed during the HEF for digesting one kilogram of COD. It can be evaluated using Eq. (2) (Ghjair & Abbar, 2023):

$$SEC = \frac{E \times I \times t \times 1000}{\left(C_o - C_f\right) \times V}, \quad (2)$$

where I denotes the current (A), E is the applied cell voltage (Volt), t symbolizes the electrolysis period (h), V indicates the volume of effluent (L). Accordingly, unit of SEC is kWh/kgCOD.

The total iron concentration was analyzed on a UV-vis spectrophotometer (Shimadzu/Japan UV-Vis spectrometer) at λ_{max} = 510 nm using the 1.10-phenanthroline method while for cerium concentration at $\lambda \approx$ 650–660 nm using the Arsenazo III method (Wang et al., 2018). BOD was determined using BOD-System BD600, Lovibond. Concentration of Phenol was determined by method 8047 of Hach Company/Hach Lange GmbH (USA), while concentration of Cl^- was identified using Photo Flex Series (WTW, model no. 14541, Germany). Total dissolved solid (TDS) was measured by using (CRISON EC-Meter, Basic 30, Spain). Turbidity was determined using turbidity meter TB 210 IR Lovibond, Germany.

3. Results and discussion

3.1. Characterization of the catalyst

3.1.1. BET and pHpzc results

The performance of HEF catalyst depends strongly on the BET and pore structure of catalyst, since these feature determine the accessibility of reactants inside the catalyst and the number of active sites (Wang et al., 2016). Table 2 presents the BET results where AC has a BET of 1247.86 m^2/g indicating its adsorption capacity. The BET of AC decreased with adding any metal oxides. It decreased to 1143.382 m^2/g with the addition of iron but decreased less with the addition of cerium to be 1207.936 m^2/g. The cooperation of both Fe and Ce leads to a lower BET than the individual case.

Additionally, increasing the Fe content while maintaining Ce content constant leads to lower BET. This can be explained by the fact that iron oxides form large particles that clog pores, reducing the diffusion of hydrogen peroxide (H_2O_2) despite the availability of more active iron sites. Furthermore, the presence of cerium (CeO_2) helps disperse iron oxides and prevent their aggregation (Keyikoğlu et al., 2022). These results confirmed the presence of Fe and Ce within the AC structure. The decrease in BET also confirmed the successful loading within the pores of the AC, not just on its outer surface. Furthermore, despite the relatively low BET reduction, the catalytic activity of the catalyst was expected to be enhanced more rapidly due to the introduction of redox active sites such as Fe(II)/Fe(III) and Ce(III)/Ce(IV), which promote the decomposition of hydrogen peroxide into hydroxyl radicals, leading to further degradation of organic pollutants (Nidheesh & Gandhimathi, 2012).

Table 2. BET and pHpzc results for AC and its loading with Fe and Ce

Catalyst	BET (m^2/g)	pH_{pzc}
AC	1247.860	6.4
AC+Fe	1143.382	7.2
AC+Ce	1207.936	7.4
AC+(Fe/Ce) (1:1)	1098.064	7.6
AC+(Fe/Ce) (2:1)	1083.962	7.7
AC+(Fe/Ce) (4:1)	1071.502	7.8

Similar behavior was observed by Tesnim et al. (2024b) in their work on preparing AC loaded with zero valent iron where BET decreased from 1314.89 m^2/g for AC alone to 652.01 m^2/g with loading Fe causing a significant decrease in the adsorption capacity of AC due to the use of polyphenols extracted from palm petioles as reducing agents

for the iron salt. Similar results have been observed in previous studies (Xiao et al., 2014; Wang et al., 2018).

Table 2 shows that pH_{pzc} increases with AC loading with iron and cerium and with increasing the basicity. This upward shift means that at pH 3 (which is more favorable for the Fenton reaction), the surface remains positively charged, resulting in a strong interaction with the negative H_2O_2, resulting in increased hydroxyl production, which stabilizes the metal sites (Wang et al., 2018). Several studies have confirmed the increase in pH_{pzc} with AC doped with metal oxides (Lu et al., 2021; Bogeat-Barroso et al., 2025; Fairuzi & Yuniarto, 2025).

3.1.2. XRD results

Figure 3 shows the XRD results for catalysts composed of AC+Fe (a) and AC+Ce (b) while Figure 4 shows the XRD results for catalysts composed of AC+Fe/Ce (1:1) (a) and AC+Fe/Ce (2:1) (b). Figure 5 represents XRD for catalyst composed of AC+Fe/Ce (4:1). In all the XRD results, no sharp peak was observed in the 2θ range (20^0–30^0), confirming that amorphous carbon is dominant (Tesnim et al., 2024b; Xiao et al., 2014; Raji et al., 2023). A zero-valent iron peak was observed in all catalysts, except AC+Ce, at 2θ of 44.7^0 (Tesnim et al., 2024b; Xiao et al., 2014; Ling et al., 2012; Ali et al., 2020; Chen et al., 2022). Wide-angle XRD (Figure 3a) indicates that the species of iron are well-distributed within AC, creating very small crystalline particles with sizes below the XRD detection limit (Xiao et al., 2014). In Figure 3b, a characteristic peak of cerium dioxide (CeO_2) was observed at 2θ of 47.01^0 (Chen et al., 2022; Ahemad et al., 2025). Peaks for Fe_2O_3 were also observed at 2θ of 35.5^0 and 74^0 (Lu et al., 2024: Huang et al., 2024). For AC+Fe/Ce (2:1), strong peaks for Fe and CeO_2 were observed at 2θ, 44.7^0 and 47.4^0, respectively, and the convergence increased with the transition at high Ce content in AC+Fe/Ce (1:1), while the Ce peak disappeared with decreasing Ce content in AC+Fe/Ce (4:1).

3.1.3. FTIR results

Figure 6 shows the FTIR results for catalysts composed of AC+Fe (a) and AC+Ce (b) while Figure 7 shows the FTIR results for catalysts composed of AC+Fe/Ce (1:1) (a), and

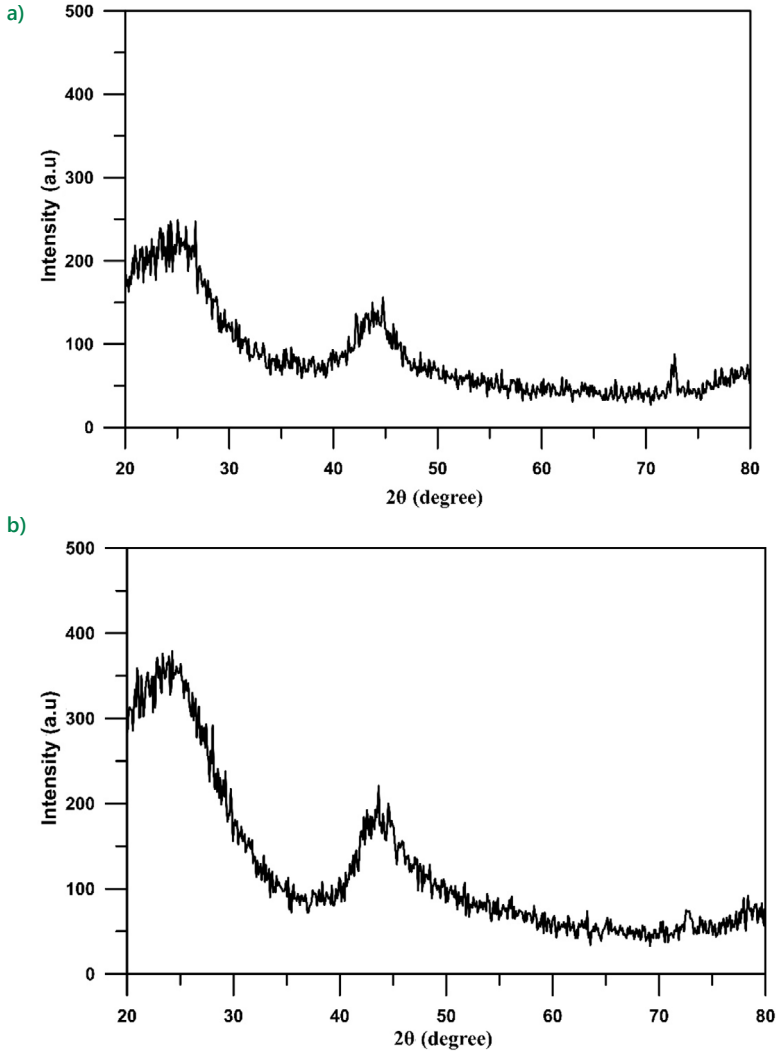

Figure 3. XRD result for HEF catalysts: a) AC+Fe; b) AC+Ce

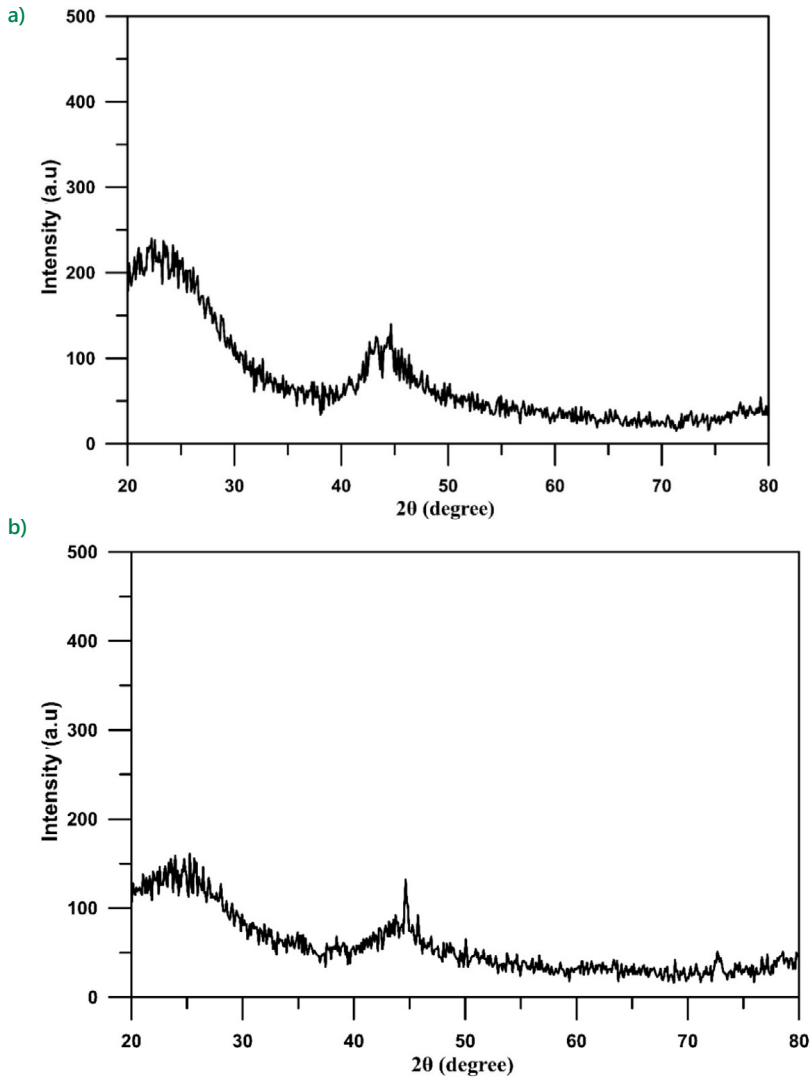

Figure 4. XRD results for the HEF catalysts: a) AC+Fe/Ce (1:1); b) AC+Fe/Ce (2:1)

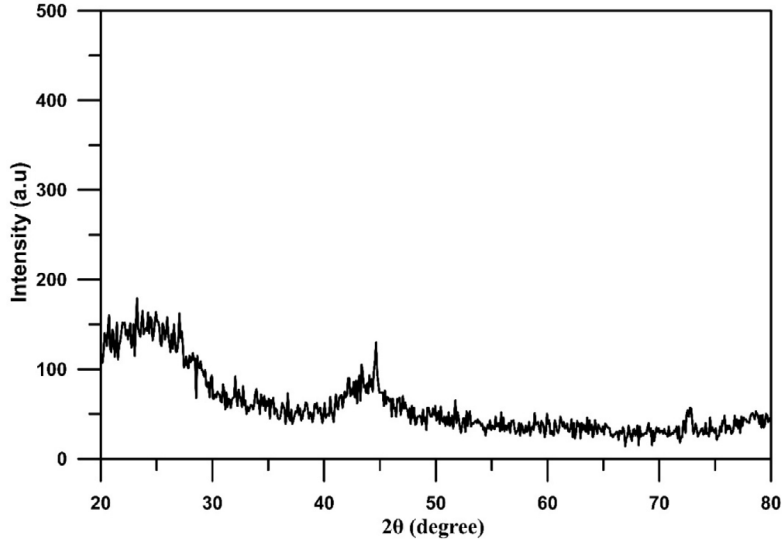

Figure 5. XRD results for the HEF catalyst AC+Fe/Ce (4:1)

AC+Fe/Ce (2:1) (b). Figure 8 represents FTIR for catalyst composed of AC+Fe/Ce (4:1). The peaks at 3767.46 and 3745.19 cm^{-1} are associated with non-hydrogen bounded, isolated surface hydroxyl group on CeO_2 as seen in the AC+Ce, AC+Fe/Ce (1:1), and AC+Fe/Ce (2:1) catalysts (Podobiński et al., 2023). The Ce-O peaks can be observed at 470–540 cm^{-1} (Farahmandjou et al., 2016). The peaks at 467.29 and 435.3 cm^{-1} are associated with Fe-O (Huang et al., 2024; Pan et al., 2019; Sun et al., 2012). The large broad bands at (3439.14, 3427.63, 3442.09, 3429.74 cm^{-1}) are belong to the O-H stretching vibration of the OH-groups (Farahmandjou et al., 2016; Dong et al., 2017). The peaks at 1689.97, 1641.12, and 1692.96 cm^{-1} are belong to C=O group (Huang et al., 2024; Dong et al., 2017). The peaks at 1577.51, 1546.94, 1579.18, and 1577.19 cm^{-1} are belong to C=C group (Huang et al., 2024; Dong et al., 2017). The C-O group was observed at 1061.51 and 1067.47 cm^{-1} (Huang et al., 2024; Dong et al., 2017). The peaks at 1383.86, 1424.63, and 1348.45 cm^{-1} are associated with the C-H group (Farahmandjou et al., 2016). FTIR results confirmed the loading of AC with iron and cerium.

3.1.4. SEM and EDS results

Figure 9 shows the SEM images for catalysts composed of AC with Fe (a) and with Ce (b) while Figure 10 shows the SEM images for catalysts composed of AC with Fe/Ce (1:1) (a), with Fe/Ce (2:1) (b), and with Fe/Ce (4:1) (c).

The results confirmed that zero-valent iron (ZVI) nanoparticles particles, as well as cerium dioxide particles, were immobilized on the surface or within the pores of AC. Immobilization of ZVI nanoparticles particles with AC appears to prevent their aggregation, thus contributing to the keep their high surface area and reactivity (Xiao et al., 2014). The EDS results are shown in Figure 11 for AC with Fe/Ce (1:1) (a), and with Fe/Ce (2:1) (b) while Figure 12 shows EDS for AC with Fe/Ce (4:1). Results confirmed the

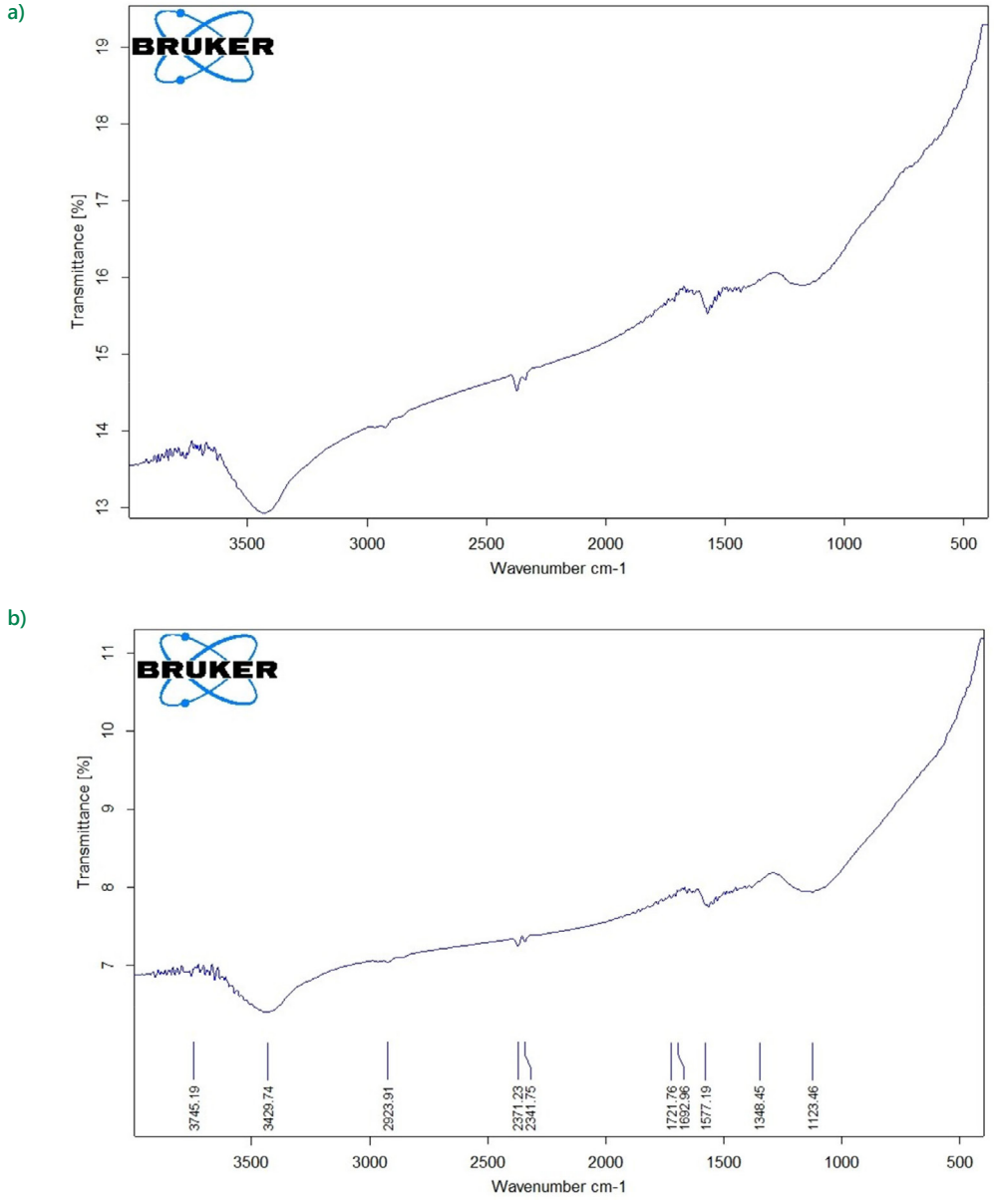

Figure 6. FTIR results for the HEF catalysts: a) AC+Fe; b) AC+Ce

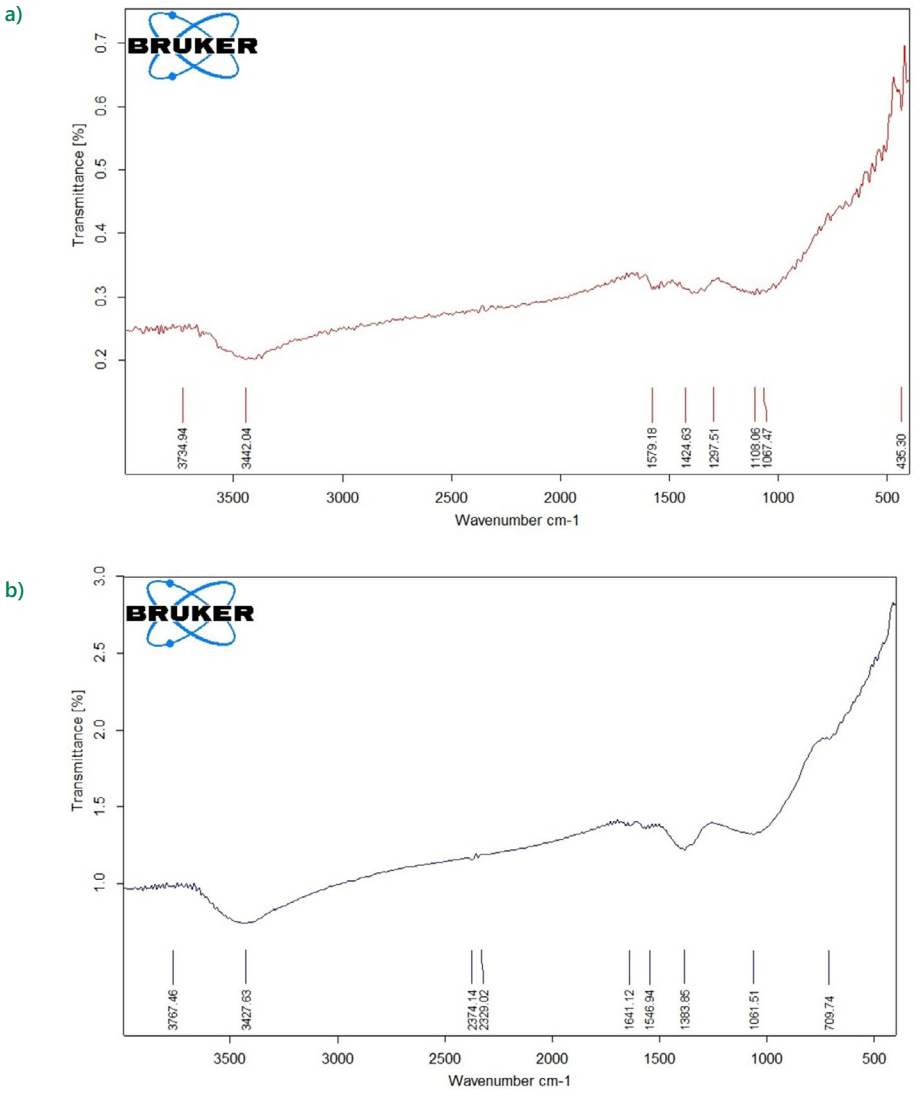

Figure 7. FTIR results for the HEF catalysts: a) AC+Fe/Ce (1:1); b) AC+Fe/Ce (2:1)

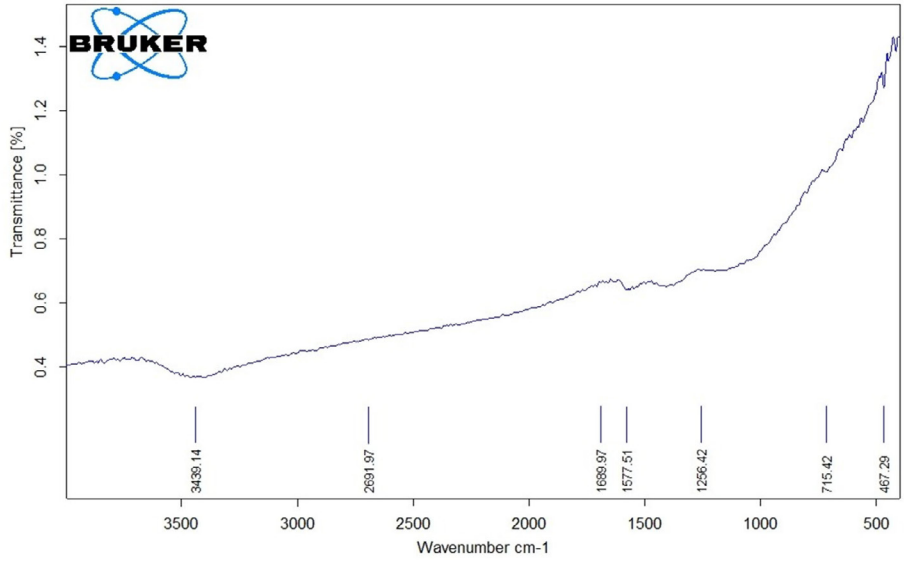

Figure 8. FTIR results for the HEF catalyst composed of AC+Fe/Ce (4:1)

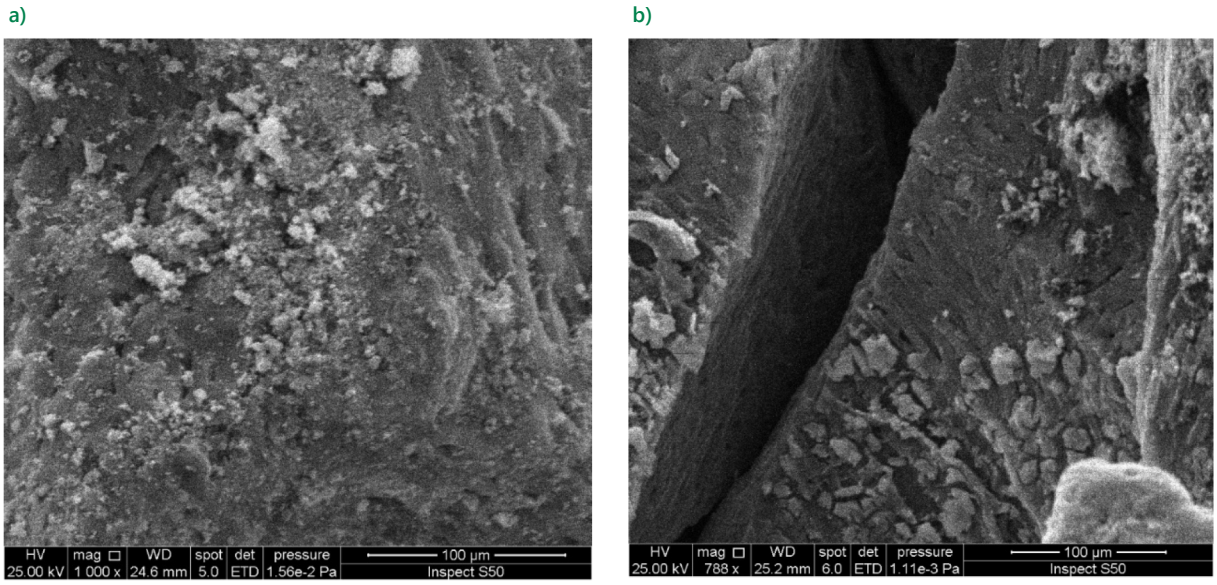

Figure 9. SEM images for the HEF catalysts: a) AC+Fe; b) AC+Ce

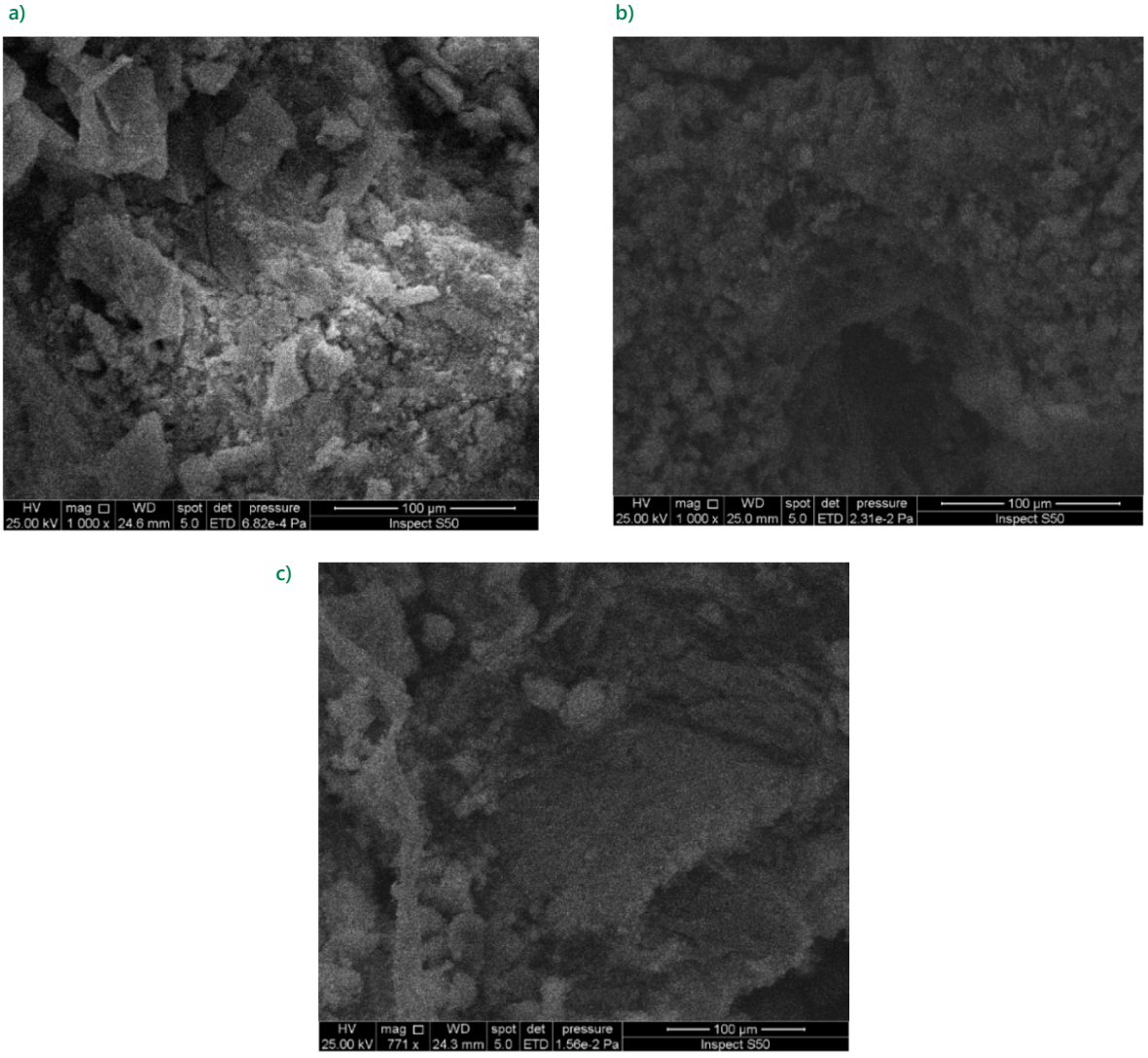

Figure 10. SEM images for the HEF catalysts: a) AC+Fe/Ce (1:1); b) AC+Fe/Ce (2:1); c) AC+Fe/Ce (4:1)

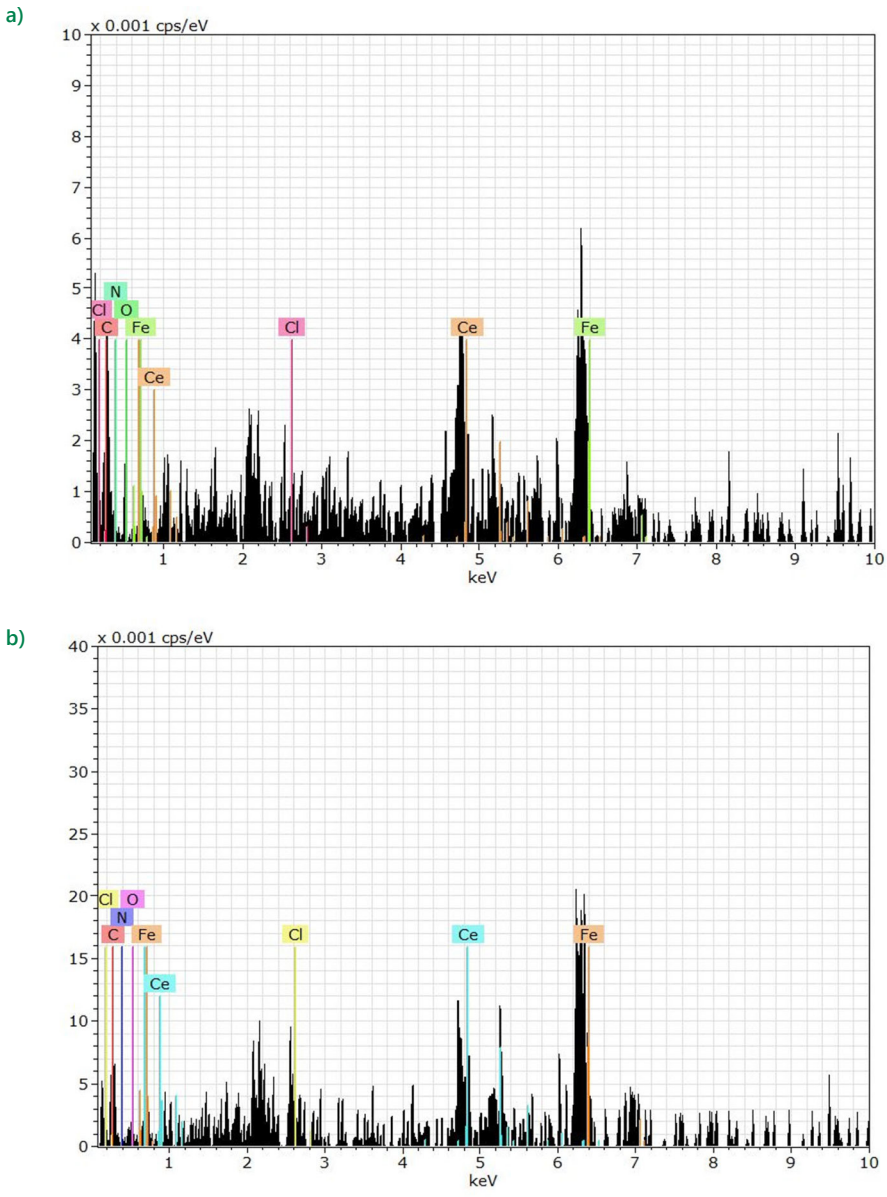

Figure 11. EDS results for the HEF catalysts: a) AC+Fe/Ce (1:1); b) AC+Fe/Ce (2:1)

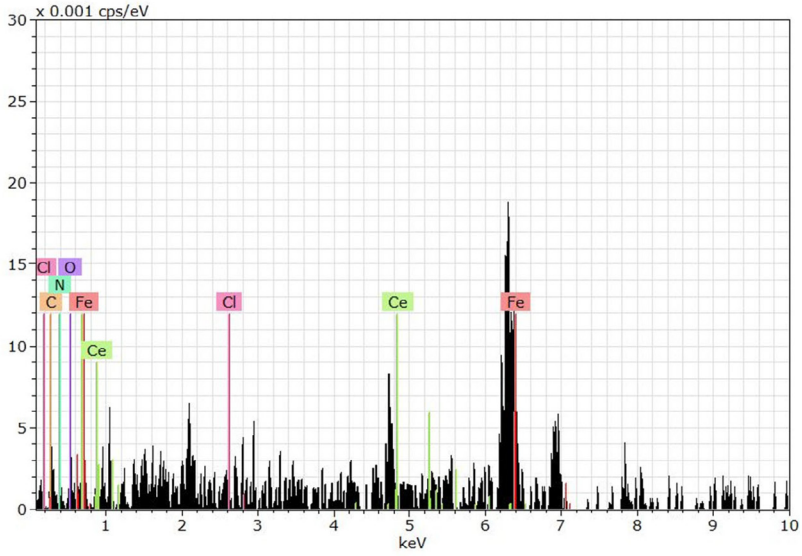

Figure 12. EDS results for the HEF catalyst composed of AC+Fe/Ce (4:1)

presence of Fe and Ce in the catalyst structures at different molar ratios. Therefore, the preparation method is suitable and successful.

3.1.5. Activity of the catalyst

The activity results are displayed in Figure 13. It was observed that using AC alone gives very low MB removal with a RE of 23%. Combining anodic oxidation with AC significantly improves the RE to 68% at an AC dosage of 0.33 g/L. This increases to 72% with increasing the AC dosage to 0.5 g/L. These results confirmed that the adsorption effect of AC to MB was weak in comparison with anodic oxidation due to generation more of OH radical on the anode from discharge of H_2O and generation of H_2O_2 on cathode from O_2 reduction that enable more oxidation of MB (Zare et al., 2024). Similar results were found by Fan et al. (2023) in degradation of MB using "Core-shell structured Fe^0/Mn^0@ Fe/Mn oxides bimetallic nanocomposites". Similar behavior was found using different pollutant (Tesnim et al., 2024b; Zare et al., 2024).

The addition of catalyst further improves the RE%, increasing up to 81% with the addition of Fe and 76.8% with the addition of Ce maintaining the same catalyst dosage (0.5 g/L). Combining Ce with Fe loading on AC further improves the RE to 84% for Fe/Ce (4:1). Further increasing the Ce content further improves the RE% to 91% for Fe/Ce (2:1). However, increasing the Ce content above Fe/Ce (2:1) has a negative effect on the RE%, which decreased to 86.8% in case of Fe/Ce (1:1). Similar results were found using AC loaded with zero valent iron (Tesnim et al., 2024b; Fan et al., 2023). It was found that AC+ Fe/Ce (2:1) gives the highest removal of MB due to the synergy resulted by Ce^{4+}/Ce^{3+} with Fe^{3+}/Fe^{2+} during the operation (Zhang et al., 2022). While the lower in degradation with further increase in Ce content could be attributed to the decreasing in H_2O_2 due to its reaction with Ce^{3+} (Xu & Wang, 2012). Results of activity confirmed that mechanism of oxidation is governed by EF with AO rather than adsorption. To support this confirmation, further experiments were conducted using three scavengers (5 mM tert-butyl alcohol (TBA), 5 mM ethanol (EtOH), and 10 mM p-benzoquinone (p-BQ) (Tesnim et al., 2024b). TBA was used to scavenge the $^{\bullet}OH$ radical, while EtOH was used to scavenge the sulfate radical ($SO_4^{\bullet-}/^{\bullet}OH$) (Hussain et al., 2017) and p-BQ to scavenge the $O_2^{\bullet-}$ (Li et al., 2016). The results are shown in Figure 14.

Results displayed that adding TBA causes a decrease in MB removal from 91% to 45.2% while adding EtOH makes a decrease in MB removal up to 55.4%. Furthermore, adding p-BQ causes a reduction in MB removal from 91 to 82%. These results confirm that oxidation by $^{\bullet}OH$ radicals is the predominant in HEF using AC+Fe/Ce (2:1) while $O_2^{\bullet-}$ radicals have a minor role in MB degradation. Several studies confirmed this behavior for HEF with heterogeneous nanoparticles (Xu et al., 2024; Sadeghi et al., 2019).

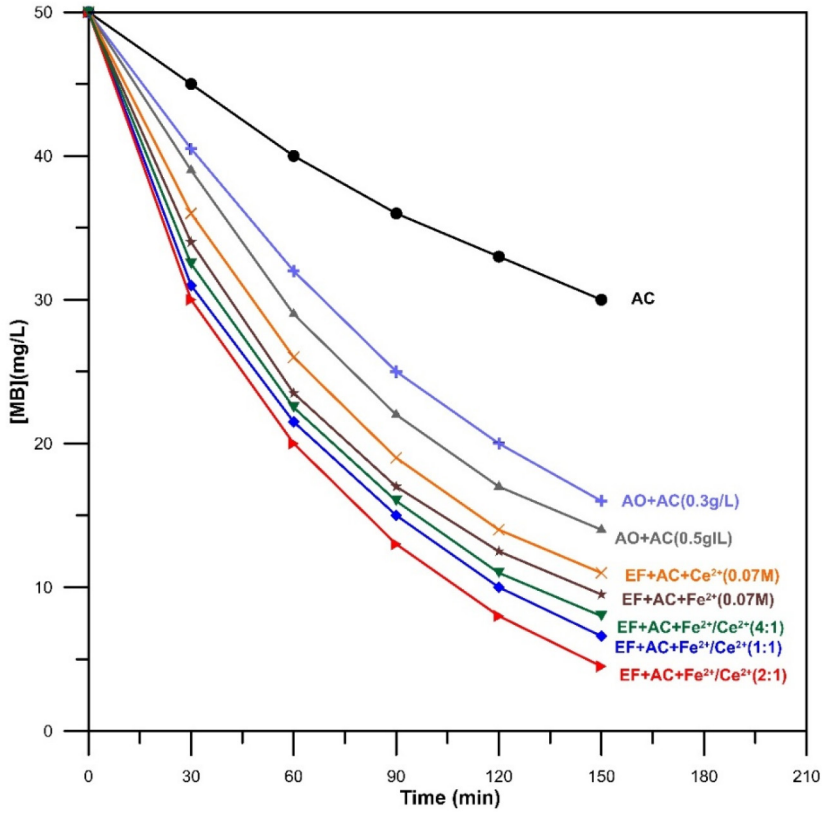

Figure 13. Results of activity test for the HEF catalyst. 50 mg/L MB, 0.1 M Na_2SO_4, 20 mA/cm^2, pH 3, 0.5 g/L catalyst, 25 ^{0}C

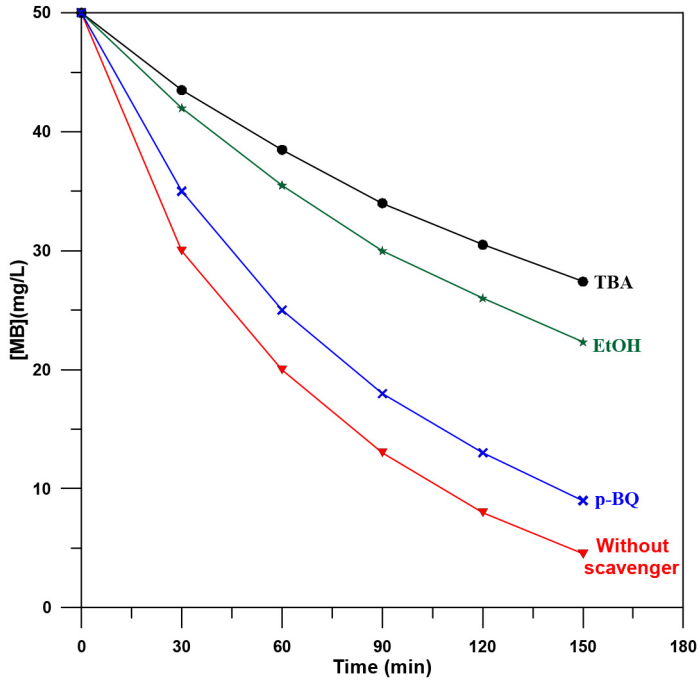

Figure 14. Effect of scavengers on degrading MB by HEF process. 50 mg/L MB, 0.1 M Na_2SO_4, 20 mA/cm^2, pH 3, 0.5 g/L catalyst, 25 ^{0}C

3.1.6. Removal of COD by the catalyst

Performance of AC+Fe/Ce (2:1) as an HEF catalyst in removal of COD from PRW was examined using a fixed amount of catalyst (1 g/L) for a period of 90 min.

Current density is a vital operating variable in HEF process since its value determined the rate of •OH generation in the anode and rate of H_2O_2 generation on the cathode (Wang et al., 2018). Figure 15 demonstrates the effect of current density on the COD decay with time. Increasing current density from 5 mA/cm^2 to 10 mA/cm^2 causes an increase in COD removal from 74.26% to 83.4%. However, further increasing in current density has a negative effect on COD removal which deceased to 80.13 at 15 mA/cm^2. The interpretation of increasing removal of COD to an

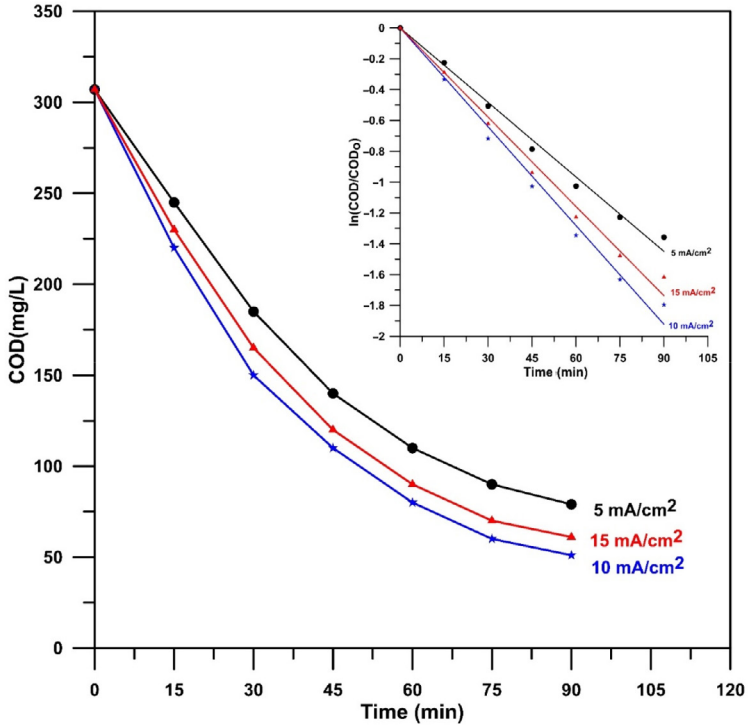

Figure 15. Impact of current density on COD decay in HEF system. Inset: ln(COD/COD$_o$)vs. time. pH = 3, 1 g/L catalyst, 0.1 M Na_2SO_4, 25 ^{0}C

optimum value as the current density increased can be explained as follows: increasing current leads to accelerate generation and accumulation of H_2O_2 as well as promoting the conversion of Fe^{3+} to Fe^{2+} on the cathode (Eq. (3)) which regenerates Fe^{2+} to catalyze the Fenton reaction (Eq. (4)) (Wang et al., 2018):

$$Fe^{3+} + e^- \rightarrow Fe^{2+}; \quad (3)$$

$$Fe^{2+} + H_2O_2 + H^+ \rightarrow Fe^{3+} + HO^{\bullet} + OH^-. \quad (4)$$

Decreasing of COD removal as the current density goes beyond 10 mA/cm^2 can interpreted as follows: by continuous increasing the current, the amount of H_2O_2 would not enhanced and brakes down causing limiting in the efficiency of Fenton reaction (Wang et al., 2018). Furthermore, excess H_2O_2 could scavenge $HO^{\bullet}$ leading to reducing amount of $HO^{\bullet}$ available for degradation the organic pollutant or transfer H_2O_2 to its radicals ($HOO^{\bullet}$) (Eq. (5)) which exhibits lower oxidation power than $HO^{\bullet}$ (Brillas & Martínez-Huitle, 2015; Oturan et al., 2011).

$$H_2O_2 + HO\bullet \rightarrow HOO\bullet + H_2O. \quad (5)$$

Similar results were found in previous studies based on AC loaded with iron (Tesnim et al., 2024b; Wang et al., 2018; Lu et al., 2024). Energy consumption increased from 3.799 to 17.987 kWh/kgCOD as the current density increased from 5 to 15 mA/cm^2

A kinetic study for removing COD by HEF was performed and result is shown as inset plot at Figure 15. It was cleared that degrading of COD obeys a pseudo first order kinetic (Eq. (6)) since R^2 for all lines are greater than 0.996 (Li et al., 2016):

$$-\frac{dCOD}{dt} = k_{app}[COD], \quad (6)$$

where k_{app} is the apparent rate constant (min^{-1})

The rate constant at 10mA/cm^2 is the higher with a value of 0.02136 min^{-1} which is higher than that observed at 5 mA/cm^2 (0.0161 min^{-1}) and 15 mA/cm^2 (0.0193 min^{-1}) confirming that speed of reaction is the highest at 10 mA/cm^2. Similar results were found in previous studies (Xu et al., 2024; Pormazar & Dalvand, 2025; Tan et al., 2023).

Figure 16 shows the effect of pH on COD decay over time at 10 mA/cm^2. Increasing pH from 3 to 7 resulted in a decrease in COD removal from 83.4% to 78.83%. Although the removal efficiency decreased as pH approached 7, its value remained high, confirming the catalyst's ability to operate close to neutral media. Acidic pH is preferred for H_2O_2 generation and anodic oxidation, which promotes the Fenton reaction. Furthermore, in acidic conditions, more Fe loss occurs from the catalyst, resulting in greater contaminant removal (Wang et al., 2018), while in alkaline conditions, H_2O_2 decomposition occurs more rapidly (Ye et al., 2023). In an alkaline media, Fe-OOH can be deposited on the AC surface, preventing the release of Fe^{2+} (Vialich et al., 2022). Studies have shown that the pH range of reaction can be expanded when using nano-zero valent iron as the iron source in HEF systems (Hou et al., 2016). Similar behavior has been observed in previous studies based on iron-loaded AC (Tesnim et al., 2024b; Wang et al., 2018; Lu et al., 2024) and studies based on nanoscale metal oxides (Mohammadi et al., 2024; Fan et al., 2023; Zare et al., 2024; Zhang et al., 2022). Energy consumption increased from 9.228 to 12.36 kWh/kgCOD as the pH

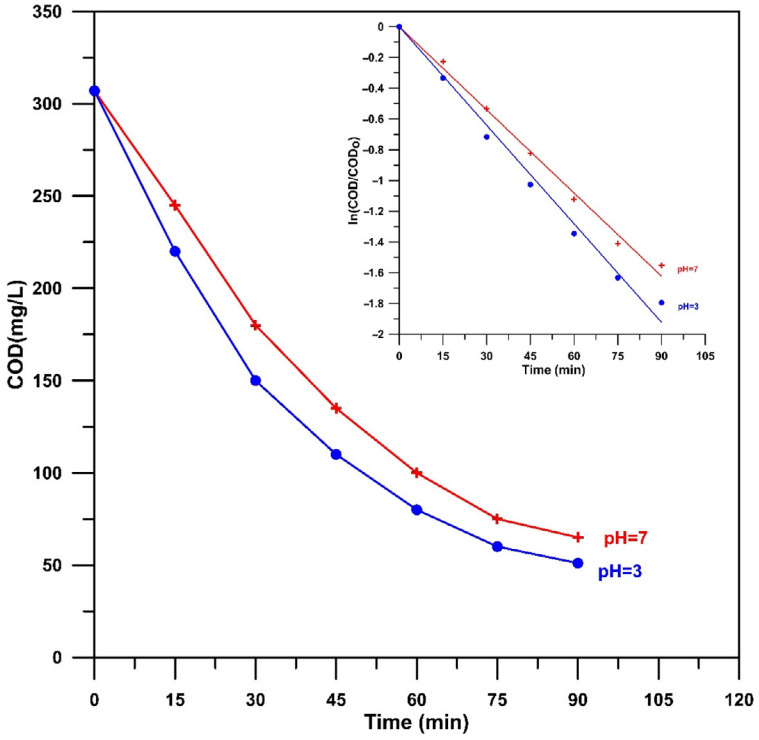

Figure 16. Impact of pH on COD decay in HEF system. Inset: ln(COD/COD$_o$)vs.time.10 mA/cm^2, 1 g/L catalyst, 0.1 M Na_2SO_4, 25 °C

Table 3. Properties of wastewater after treatment by HEF

Property	TDS	Phenol	COD	BOD	Cl^-	Turbidity
Value	396 mg/L	0.08 mg/L	51 mg/L	35 mg/L	450 mg/L	3.1 NTU

increased from 3 to 7. The increased SEC with increasing pH can be attributed to increased $Fe(OH)_3$ precipitation, non-productive decomposition of hydrogen peroxide with increasing pH, and decreased cathodic efficiency, where oxygen is reduced to water rather than to H_2O_2 at a significant rate with increasing the pH. All of these factors reduce removal efficiency and increase cell resistance, resulting in increased SEC (Oturan & Aaron, 2014). R^2 for all lines of ln (COD/CODo) verses time are higher than 0.996. Furthermore, the rate constant at pH 3 has a value of 0.02136 min^{-1} which is higher than that observed at pH of 7 (0.0180 min^{-1}) confirming that speed of reaction is higher at acidic conditions. Similar results were found in previous studies (Xu et al., 2024; Tan et al., 2023; Tesnim et al., 2024b; Pormazar & Dalvand, 2025).

Table 3 shows the properties of wastewater treated at 10 mA/cm^2, pH =3, and 1 g/L catalyst. It was found that, in addition to removing COD, BOD was removed by 75%, phenol by 99.56%, and turbidity by 91.1%. This confirms the ability of the prepared catalyst to treat and discharge wastewater within environmentally safe limits.

3.4. Reusability of catalyst

From an industrial application perspective, the stability and long-term reusability of a catalyst play a key role in evaluating the process efficiency. In this research, the stability of the HEF catalyst was investigated by running the treatment system sequentially for several cycles. Each time, the catalyst was cleaned with distilled water, then ethanol, then left in an oven overnight, and then used for the next cycle. This process was repeated for different cycles until the COD removal efficiency decreased. Figure 17 shows the RE% at different operating cycles under the following conditions: 10 mA/cm^2, pH = 3, and 1 g/L catalyst. The RE% decreased from 83.4% to 78.5% after the fifth run, confirming the effectiveness of the HEF catalyst in removing COD from PRW. The decline in removal efficiency could be attributed to buildup of intermediates and sludge on the surface of catalyst.

Iron leaching was found to be 0.4 mg/L after five cycles, which is lower than the permissible level based on EU emissions (less than 2 mg/L) (Wang et al., 2018), while cerium leaching was 0.12 mg/L. The results confirm that the catalyst is catalytically stable and environmentally friendly, with iron leaching less than 2 mg/L and cerium leaching less than 0.5 mg/L (Zárate-Guzmán et al., 2019).

3.5. Comparison with similar studies

A comparison was made with works involving treatment of different real wastewaters using different heterogeneous electro Fenton as shown in Table 4. The present work could be consider efficient in treatment a complex wastewater such as petroleum refineries in a suitable operating time with a suitable catalyst dosage combined with lower energy consumption. Furthermore using graphite material in construction of the cell electrodes gives further economic advantage in comparison with those electrodes mentioned in Table 4. Overall, the present system could be considered as a promising approach for treating petroleum refinery wastewaters.

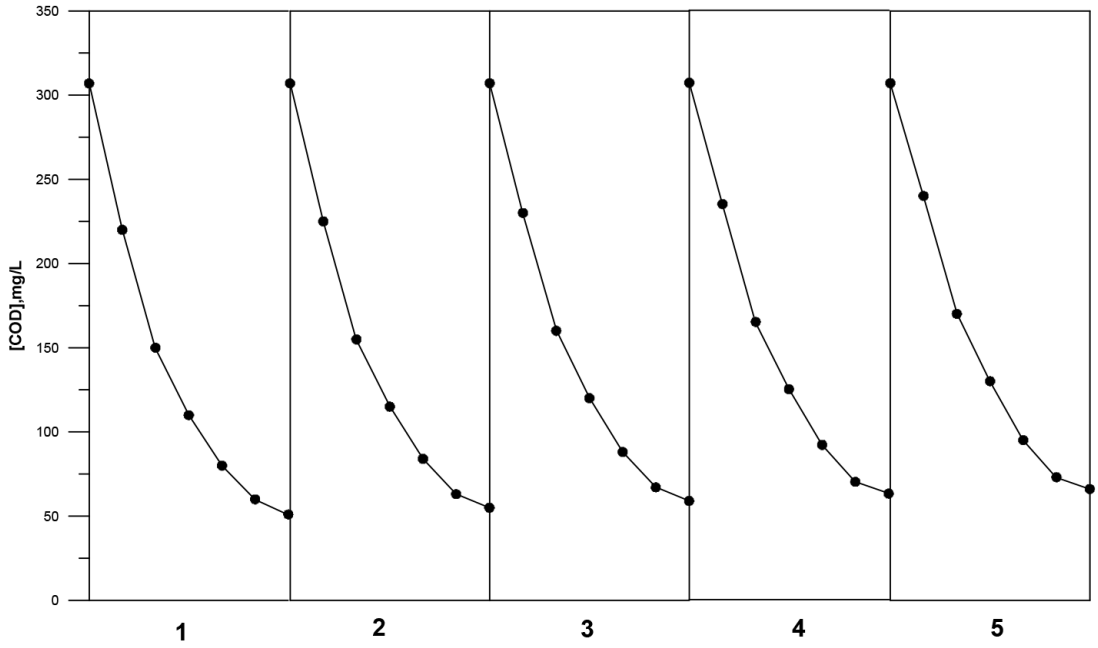

Figure 17. Reusability of HEF. 10 mA/cm^2, pH = 3, and 1 g/L catalyst

Table 4. Comparison with related works

Wastewater type	HEF catalyst	Electrodes and conditions	Results	References
Coking factory	AC-NZVI	Anode (DSA), Cathode (Fe/AC/Ni), $[COD]_o$ = 2970.24 mg/L, 10 V, pH = 3.88, Time 360 min, 25 ^{0}C	88.91–96.65% (COD)	Meng et al. (2022)
Textile factory	MIL-8A(Fe)/ rGO	Anode (graphite), Cathode (titanium), $[COD]_o$ = 2150mg/L, Time 60 min, 0.61 g/L catalyst, 0.9 mA/cm^2, pH = 5, 25 ^{0}C	78% (COD), 3.67 kWh/g COD	Esmaili et al. (2025)
Municipal wastewater Antipyrine	AC-NZVI	Anode (BDD), Cathode (carbon felt), ($[ATP]_o$ = 40 mg/L, Time 150 min, 55 mA/cm^2, pH = 7, 25 ^{0}C	75 % (TOC)	Tesnim et al. (2024a)
Diclofenac	MSWCNTs	Anode (RuO_2/Ti), Cathode (graphite felt) Time 120 min, 80 mg/L catalyst, 5 mA/cm^2, pH = 5($[DCF]_o$ = 10 mg/L, 25 ^{0}C	71.12% (COD)	Sadeghi et al. (2019)
Wastewater (pesticide factory)	zeolite Y-nZVI	Anode (SS 316), Cathode (graphite), 272 mA, pH = 3, 1.78 g catalyst, Time 125 min, $[COD]_o$ = 1123 mg/L, 25 ^{0}C	91.26 % (COD)	Mohammadi et al. (2024)
Neonicotinoid wastewater	NZVI-BC	Anode (RuO_2/Ti), Cathode (carbon fabric), 150 mA, pH = 9, 0.3 g catalyst, Time 120 min, $[CLO]_o$ = 50 mg/L, 25 ^{0}C	96.9% clothianidin (CLO)	Zhang et al. (2020)
Petroleum refinery	AC+Fe/Ce (2:1)	Anode (graphite), Cathode (MPGAD), 10 mA/cm^2, pH = 3, Time 90 min, 1 g/L catalyst, $[COD]_o$ = 307 mg/L, 25 ^{0}C	83.4% (COD) 9.228 kWh/kg COD	Present work

4. Conclusions

In the present work, a novel HEF catalyst consisting of AC loaded with Fe/Ce at different molar ratios was successfully prepared using a one-step reduction method. The composite catalyst exhibited excellent catalytic performance for MB decomposition. The good performance was attributed to the synergistic effect between Ce^{4+}/Ce^{3+} and Fe^{3+}/Fe^{2+} conversion. A higher MB removal rate of 91% was achieved within 150 min using an HEF catalyst composed of AC loaded with Fe/Ce at a molar ratio of (2:1) and operating at 20 mA/cm^2 with pH = 3. Electrochemical oxidation (including EF and AO) was the main mechanism for MB removal using the AC+Fe/Ce (2:1) catalyst. The AC+Fe/Ce (2:1) catalyst was used to remove COD from PRW. COD removal of 83.4% was achieved at a current density of 10 mA/cm^2, pH of 3, and a catalyst dosage of 1 g/L, with an energy consumption of 9.22 kWh/kg COD. The prepared catalyst exhibits good performance even under neutral conditions. Reusability testing showed good catalytic activity of AC+Fe/Ce (2:1) where COD removal decreased by 5.87% after five cycles. In addition, the degradation of COD over time was found to follow pseudo-first-order kinetics for all current density and pH conditions indicating that the formation of hydroxyl radicals during the HEF system is sufficiently constant and thus provides stable and reproducible degradation performance. Therefore, AC-assisted Fe and Ce could be considered as a promising catalyst for treating various types of wastewater using HEF process. However, the present catalyst may face several limitations in its industrial application, such as the partial leaching of iron and cerium under acidic conditions, and the treatment of wastewater containing competing ions such as carbonate, which may inhibit the formation of hydroxyl radicles or act as free radical scavengers. These limitations should be addressed through pilot scale studies.

Acknowledgements

The authors thank the employees of the Department of Chemical Engineering, Baghdad University for their valuable assistance in completing this work.

References

Ahemad, H. I., Patil, G. E., Aher, Y. B., Malik, M. S., Sonawane, L. D., More, M. A., Mandawade, A. S., Patil, D. Y., Shinde, S. D., & Jain, G. H. (2025). Synthesis and characterization of CeO_2 nanoparticles using *Plectranthus barbatus* leaf extract and its CO gas sensing and antimicrobial activity. *Materials Letters*, *379*, Article 137652. https://doi.org/10.1016/j.matlet.2024.137652

Ai, Z., Gao, Z., Zhang, L., He, W., & Yin, J. J. (2013). Core–shell structure dependent reactivity of Fe@ Fe_2O_3 nanowires on aerobic degradation of 4-chlorophenol. *Environmental Science & Technology*, *47*(10), 5344–5352. https://doi.org/10.1021/es4005202

Ali, I., Afshinb, S., Poureshgh, Y., Azari, A., Rashtbari, Y., Feizizadeh, A., Hamzezadeh, A., & Fazlzadeh, M. (2020). Green preparation of activated carbon from pomegranate peel coated with zero-valent iron nanoparticles (nZVI) and isotherm and kinetic studies of amoxicillin removal in water. *Environmental Science and Pollution Research*, *27*(29), 36732–36743. https://doi.org/10.1007/s11356-020-09310-1

Amin, M. M., Yousefinejad, S., Dehghani, M., & Rahimi, S. (2019). Catalytic effect of Fe@ Fe_2 O_3 nanowires and Fenton process on carbamazepine removal from aqueous solutions using response surface methodology. *Global Journal of Environmental Science & Management* (*GJESM*), *5*(2), 213–224. https://doi.org/10.22034/gjesm.2019.02.07

Atiyah, Z. Y., Muallah, S. K., & Abbar, A. H. (2024). Removal of COD from petroleum refinery wastewater by adsorption using

activated carbon derived from avocado plant. *South African Journal of Chemical Engineering*, *48*(1), 467–483. https://doi.org/10.1016/j.sajce.2024.03.015

Azizi, J., & Davarnejad, R. (2023). Electro-Fenton technique associated with core-shell Fe@ Fe_2O_3 nanoparticles-bentonite catalyst for pre-treating a super-pollutant industrial wastewater. *Journal of Water Process Engineering*, *51*, Article 103385. https://doi.org/10.1016/j.jwpe.2022.103385

Barhoumi, N., Olvera-Vargas, H., Oturan, N., Huguenot, D., Gadri, A., Ammar, S., Brillas, E., & Oturan, M. A. (2017). Kinetics of oxidative degradation/mineralization pathways of the antibiotic tetracycline by the novel heterogeneous electro-Fenton process with solid catalyst chalcopyrite. *Applied Catalysis B: Environmental*, *209*, 637–647. https://doi.org/10.1016/j.apcatb.2017.03.034

Bogeat-Barroso, A., Alexandre-Franco, M. F., Fernández-González, C., & Serrano, V. G. (2025). Support surface chemistry evolution during the preparation of metal oxide–activated carbon catalysts by wet impregnation: A FT-IR spectroscopy analysis. *Compounds*, *5*(3), Article 36. https://doi.org/10.3390/compounds5030036

Brillas, E., & Martínez-Huitle, C. A. (2015). Decontamination of wastewaters containing synthetic organic dyes by electrochemical methods. An updated review. *Applied Catalysis B: Environmental*, *166*, 603–643. https://doi.org/10.1016/j.apcatb.2014.11.016

Chen, J., Wan, J., Li, C., Wei, Y., & Shi, H. (2022). Synthesis of novel Fe^0-Fe_3O_4/CeO_2/C composite cathode for efficient heterogeneous electro-Fenton degradation of ceftriaxone sodium. *Journal of Hazardous Materials*, *437*, Article 129393. https://doi.org/10.1016/j.jhazmat.2022.129393

Chen, Y. P., Yang, L. M., Chen, J. P., & Zheng, Y. M. (2019). Electrospun spongy zero-valent iron as excellent electro-Fenton catalyst for enhanced sulfathiazole removal by a combination of adsorption and electro-catalytic oxidation. *Journal of Hazardous Materials*, *371*, 576–585. https://doi.org/10.1016/j.jhazmat.2019.03.043

Compton, P., Dehkordi, N. R., Casanova, P. L., & Alshawabkeh, A. N. (2023). Activated carbon modifications for heterogeneous Fenton-like catalysis. *Journal of Chemical Engineering and Catalysis*, *1*(2), 1–19. https://doi.org/10.17303/jcec.2023.2.103

Deylami, S., Sabzevari, M. H., Ghaedi, M., Azqhandi, M. A., & Marahel, F. (2023). Efficient photodegradation of disulfine blue dye and Tetracycline over Robust and Green g-CN/Ag_3VO_4/PAN nanofibers: Experimental design, RSM, RBF-NN and ANFIS modeling. *Process Safety and Environmental Protection*, *169*, 71–81. https://doi.org/10.1016/j.psep.2022.10.080

Dong, H., Deng, J., Xie, Y., Zhang, C., Jiang, Z., Cheng, Y., Hou, K., & Zeng, G. (2017). Stabilization of nanoscale zero-valent iron (nZVI) with modified biochar for Cr (VI) removal from aqueous solution. *Journal of Hazardous Materials*, *332*, 79–86. https://doi.org/10.1016/j.jhazmat.2017.03.002

Elmobarak, W. F., Hameed, B. H., Almomani, F., & Abdullah, A. Z. (2021). A review on the treatment of petroleum refinery wastewater using advanced oxidation processes. *Catalysts*, *11*(7), Article 782. https://doi.org/10.3390/catal11070782

Esmaili, F., Hasheminejad, H., & Mousaabadi, K. Z. (2025). Investigating textile wastewater treatment by electro-Fenton method with Fe-MIL-88 (A) catalyst composited with graphene oxide. *Water Resources and Industry*, *34*, Article 100302. https://doi.org/10.1016/j.wri.2025.100302

Fahim, A. S., & Abbar, A. H. (2020). Treatment of petroleum refinery wastewater by electro-Fenton process using porous graphite electrodes. *Egyptian Journal of Chemistry*, *63*(12), 4805–4819. https://doi.org/10.21608/ejchem.2020.28148.2592

Fairuzi, I. I., & Yuniarto, A. (2025). Determination Point of Zero Charge (PZC) of nZVI-MXene Adsorbent for Reduction of Ciprofloxacin Contaminants in Wastewater. *Jurnal Serambi Engineering*, *10*(2). https://jse.serambimekkah.id/index.php/jse/article/view/814

Fan, L., Wang, X., Miao, J., Cai, J., Chen, F., Chen, W., Luo, H., Cheng, L., An, X., Zhang, X., Zhang, K., & Ma, D. (2023). Core-shell structured Fe^0/Mn^0@ Fe/Mn oxides bimetallic nanocomposites as novel heterogeneous electro-Fenton catalysts for methylene blue removal. *Journal of Molecular Liquids*, *383*, Article 122069. https://doi.org/10.1016/j.molliq.2023.122069

Farahmandjou, M., Zarinkamar, M., & Firoozabadi, T. P. (2016). Synthesis of Cerium Oxide (CeO_2) nanoparticles using simple CO-precipitation method. *Revista mexicana de física*, *62*(5), 496–499.

Fayazi, M., & Ghanei-Motlagh, M. (2020). Electrochemical mineralization of methylene blue dye using electro-Fenton oxidation catalyzed by a novel sepiolite/pyrite nanocomposite. *International Journal of Environmental Science and Technology*, *17*(11), 4541–4548. https://doi.org/10.1007/s13762-020-02749-2

Ghjair, A. Y., & Abbar, A. H. (2023). Applications of advanced oxidation processes (Electro-Fenton and sono-electro-Fenton) for COD removal from hospital wastewater: Optimization using response surface methodology. *Process Safety and Environmental Protection*, *169*, 481–492. https://doi.org/10.1016/j.psep.2022.11.039

GilPavas, E., & Correa-Sanchez, S. (2019). Optimization of the heterogeneous electro-Fenton process assisted by scrap zero-valent iron for treating textile wastewater: Assessment of toxicity and biodegradability. *Journal of Water Process Engineering*, *32*, Article 100924. https://doi.org/10.1016/j.jwpe.2019.100924

Guo, J., Song, G., Zhang, X., & Zhou, M. (2023). Transition metal catalysts in the heterogeneous electro-Fenton process for organic wastewater treatment: A review. *Environmental Science: Water Research & Technology*, *9*(10), 2429–2445. https://doi.org/10.1039/D3EW00302G

Hilsendeger, L. R., Domingos, D. G., Dalari, B. L. S. K., Dalalibera, A., & Nagel-Hassemer, M. E. (2025). Treatment of textile industry effluents by Fenton processes using galvanising industry residues. *International Journal of Environment and Waste Management*, *36*(4), 419–437. https://doi.org/10.1504/IJEWM.2025.144992

Hou, B., Han, H., Jia, S., Zhuang, H., Xu, P., & Li, K. (2016). Three-dimensional heterogeneous electro-Fenton oxidation of biologically pretreated coal gasification wastewater using sludge derived carbon as catalytic pArticle electrodes and catalyst. *Journal of the Taiwan Institute of Chemical Engineers*, *60*, 352–360. https://doi.org/10.1016/j.jtice.2015.10.032

Huang, D., Liu, J., Zhang, J., Chen, Z., Zhou, Z., Xu, B., & Wang, M. (2024). Enhanced removal of florfenicol by distributing nanoscale zerovalent iron onto activated carbon: Mechanism and toxicity evaluation. *Chemical Engineering Journal*, *479*, Article 147938. https://doi.org/10.1016/j.cej.2023.147938

Hussain, I., Li, M., Zhang, Y., Li, Y., Huang, S., Du, X., Liu, G., Hayat, W., & Anwar, N. (2017). Insights into the mechanism of persulfate activation with nZVI/BC nanocomposite for the degradation of nonylphenol. *Chemical Engineering Journal*, *311*, 163–172. https://doi.org/10.1016/j.cej.2016.11.085

Jiad, M. M., & Abbar, A. H. (2023a). Treatment of petroleum refinery wastewater by sono Fenton process utilizing the in-situ generated hydrogen peroxide. *Al-Khwarizmi Engineering Journal*, *19*(2), 52–67. https://doi.org/10.22153/kej.2023.04.002

Jiad, M. M., & Abbar, A. H. (2023b). Treatment of petroleum refinery wastewater by electrofenton process using a low cost porous graphite air-diffusion cathode with a novel design. *Chemical Engineering Research and Design*, 193, 207–221. https://doi.org/10.1016/j.cherd.2023.03.021

Jinisha, R., Gandhimathi, R., Ramesh, S. T., Nidheesh, P. V., & Velmathi, S. (2018). Removal of rhodamine B dye from aqueous solution by electro-Fenton process using iron-doped mesoporous silica as a heterogeneous catalyst. *Chemosphere*, *200*, 446–454. https://doi.org/10.1016/j.chemosphere.2018.02.117

Keyikoğlu, R., Khataee, A., Orooji, Y., & Kobya, M. (2022). Synergistic effect of Fe and Co metals for the enhanced activation of hydrogen peroxide in the heterogeneous electro-Fenton process by Co-doped ZnFe layered double hydroxide. *Journal of Environmental Chemical Engineering*, *10*(6), Article 108875. https://doi.org/10.1016/j.jece.2022.108875

Kumari, P., & Kumar, A. (2023). Advanced oxidation process: A remediation technique for organic and non-biodegradable pollutant. *Results in Surfaces and Interfaces*, *11*, Article 100122. https://doi.org/10.1016/j.rsurfi.2023.100122

Li, D., Jia, J., Zheng, T., Cheng, X., & Yu, X. (2016). Construction and characterization of visible light active Pd nano-crystallite decorated and CNS-co-doped TiO_2 nanosheet array photoelectrode for enhanced photocatalytic degradation of acetylsalicylic acid. *Applied Catalysis B*: *Environmental*, *188*, 259–271. https://doi.org/10.1016/j.apcatb.2016.02.019

Li, Q., Chen, Z., Wang, H., Yang, H., Wen, T., Wang, S., Hu, B., & Wang, X. (2021). Removal of organic compounds by nanoscale zero-valent iron and its composites. *Science of the Total Environment*, *792*, Article 148546. https://doi.org/10.1016/j.scitotenv.2021.148546

Ling, X., Li, J., Zhu, W., Zhu, Y., Sun, X., Shen, J., Han, W., & Wang, L. (2012). Synthesis of nanoscale zero-valent iron/ordered mesoporous carbon for adsorption and synergistic reduction of nitrobenzene. *Chemosphere*, *87*(6), 655–660. https://doi.org/10.1016/j.chemosphere.2012.02.002

Liu, Y., Zhu, J., Chi, M., Van Eygen, G., Guan, K., & Matsuyama, H. (2025). Comprehensive review of nanofiltration membranes for efficient resource recovery from textile wastewater. *Chemical Engineering Journal*, *506*, Article 160132. https://doi.org/10.1016/j.cej.2025.160132

Lu, G., Ma, Y., Zang, L., Sun, Y., Yu, F., & Xue, R. (2021). Effects of granular activated carbon and Fe-modified granular activated carbon on anammox process start-up. *RSC Advances*, *11*(18), 10625–10634. https://doi.org/10.1039/D1RA00384D

Lu, Y., Feng, M., & Wang, Y. (2024). Enhancing the heterogeneous electro-Fenton degradation of methylene blue using sludge-derived biochar-loaded nano zero-valent iron. *Journal of Water Process Engineering*, *59*, Article 104980. https://doi.org/10.1016/j.jwpe.2024.104980

Luo, T., Feng, H., Tang, L., Lu, Y., Tang, W., Chen, S., Yu, J., Xie, Q., Ouyang, X., & Chen, Z. (2020). Efficient degradation of tetracycline by heterogeneous electro-Fenton process using Cu-doped Fe@ Fe_2O_3: Mechanism and degradation pathway. *Chemical Engineering Journal*, *382*, Article 122970. https://doi.org/10.1016/j.cej.2019.122970

Majlesi, M., & Hashempour, Y. (2017). Removal of 4-chlorophenol from aqueous solution by granular activated carbon/nanoscale zero valent iron based on Response Surface Modeling. *Archives of Environmental Protection*, *43*(4), 13–25. https://doi.org/10.1515/aep-2017-0035

Meng, G., Jiang, N., Wang, Y., Zhang, H., Tang, Y., Lv, Y., & Bai, J. (2022). Treatment of coking wastewater in a heterogeneous electro-Fenton system: Optimization of treatment parameters, characterization, and removal mechanism. *Journal of Water Process Engineering*, *45*, Article 102482. https://doi.org/10.1016/j.jwpe.2021.102482

Mirzaei, A., Chen, Z., Haghighat, F., & Yerushalmi, L. (2017). Removal of pharmaceuticals from water by homo/heterogonous Fenton-type processes–a review. *Chemosphere*, *174*, 665–688. https://doi.org/10.1016/j.chemosphere.2017.02.019

Mohammadi, M., Davarnejad, R., & Sillanpää, M. (2024). A novel catalyst based on zero-valent iron nanoparticles for assisting electro-Fenton process applied to a toxic wastewater. *Results in Engineering*, *24*, Article 102938. https://doi.org/10.1016/j.rineng.2024.102938

Nidheesh, P. V., & Gandhimathi, R. (2012). Trends in electro-Fenton process for water and wastewater treatment: An overview. *Desalination*, *299*, 1–15. https://doi.org/10.1016/j.desal.2012.05.011

Nidheesh, P. V., & Gandhimathi, R. (2014). Comparative removal of rhodamine B from aqueous solution by electro-Fenton and electro-Fenton-like processes. *CLEAN–Soil*, *Air*, *Water*, *42*(6), 779–784. https://doi.org/10.1002/clen.201300093

Oturan, M. A., & Aaron, J. J. (2014). Advanced oxidation processes in water/wastewater treatment: Principles and applications. A review. *Critical Reviews in Environmental Science and Technology*, *44*(23), 2577–2641. https://doi.org/10.1080/10643389.2013.829765

Oturan, M. A., Oturan, N., Edelahi, M. C., Podvorica, F. I., & El Kacemi, K. (2011). Oxidative degradation of herbicide diuron in aqueous medium by Fenton's reaction based advanced oxidation processes. *Chemical Engineering Journal*, *171*(1), 127–135. https://doi.org/10.1016/j.cej.2011.03.072

Pan, L., Cao, Y., Zang, J., Huang, Q., Wang, L., Zhang, Y., Fan, S., Tang, J., & Xie, Z. (2019). Preparation of iron-loaded granular activated carbon catalyst and its application in tetracycline antibiotic removal from aqueous solution. *International Journal of Environmental Research and Public Health*, *16*(13), Article 2270. https://doi.org/10.3390/ijerph16132270

Patil, A. D., & Raut, P. D. (2014). Treatment of textile wastewater by Fenton's process as a Advanced Oxidation Process. *IOSR Journal of Environmental Science*, *Toxicology and Food Technology*, *8*, 29–32. https://doi.org/10.9790/2402-081032932

Podobiński, J., Zimowska, M., Śliwa, M., & Datka, J. (2023). IR studies of ethoxy groups on CeO2. *Molecules*, *28*(3), Article 1251. https://doi.org/10.3390/molecules28031251

Pormazar, S. M., & Dalvand, A. (2025). Heterogeneous electro-Fenton process using a novel catalytic electrode for the degradation of direct dye from aqueous solutions: Modeling, optimization, degradation pathway and toxicity evaluation. *Applied Water Science*, *15*(3), Article 52. https://doi.org/10.1007/s13201-025-02394-5

Pournamdari, E., Niknam, L., Davoudi, S., & Khazali, F. (2024). Response surface methodology, and artificial neural network model for removal of textile dye Reactive Yellow 105 from wastewater using Zeolitic Imidazolate-67 modified by Fe_3O_4 nanoparticles. *International Journal of Phytoremediation*, *26*(1), 98–113. https://doi.org/10.1080/15226514.2023.2226217

Raji, Y., Nadi, A., Mechnou, I., Saadouni, M., Cherkaoui, O., & Zyade, S. (2023). High adsorption capacities of crystal violet dye by low-cost activated carbon prepared from Moroccan Moringa oleifera wastes: Characterization, adsorption and mechanism study. *Diamond and Related Materials*, *135*, Article 109834. https://doi.org/10.1016/j.diamond.2023.109834

Sadeghi, M., Mehdinejad, M. H., Mengelizadeh, N., Mahdavi, Y., Pourzamani, H., Hajizadeh, Y., & Zare, M. R. (2019). Degradation of diclofenac by heterogeneous electro-Fenton process

using magnetic single-walled carbon nanotubes as a catalyst. *Journal of Water Process Engineering*, *31*, Article 100852. https://doi.org/10.1016/j.jwpe.2019.100852

Sadek, N. J., Alradhi, S. M., Albayati, T. M., Salih, I. K., & Elmi Fard, N. (2025). Recent developments in petroleum wastewater treatment based on advanced oxidation processes: A review. *Iranian Journal of Chemistry and Chemical Engineering*, *44*(4), 1089–1120. https://doi.org/10.30492/ijcce.2025.2044930.6870

Sánchez-Sánchez, C. M., Expósito, E., Casado, J., & Montiel, V. (2007). Goethite as a more effective iron dosage source for mineralization of organic pollutants by electro-Fenton process. *Electrochemistry Communications*, *9*(1), 19–24. https://doi.org/10.1016/j.elecom.2006.08.023

Sathya, K., Nagarajan, K., Carlin Geor Malar, G., Rajalakshmi, S., & Raja Lakshmi, P. (2022). A comprehensive review on comparison among effluent treatment methods and modern methods of treatment of industrial wastewater effluent from different sources. *Applied Water Science*, *12*(4), Article 70. https://doi.org/10.1007/s13201-022-01594-7

Soufi, A., Hajjaoui, H., Elmoubarki, R., Abdennouri, M., Qourzal, S., & Barka, N. (2021). Spinel ferrites nanoparticles: Synthesis methods and application in heterogeneous Fenton oxidation of organic pollutants–A review. *Applied Surface Science Advances*, *6*, Article 100145. https://doi.org/10.1016/j.apsadv.2021.100145

Sun, H., Zhou, G., Liu, S., Ang, H. M., Tadé, M. O., & Wang, S. (2012). Nano-Fe^0 encapsulated in microcarbon spheres: Synthesis, characterization, and environmental applications. *ACS Applied Materials & Interfaces*, *4*(11), 6235–6241. https://doi.org/10.1021/am301829u

Sun, Y., Tu, S., Li, Y., Sui, X., Geng, S., Wang, H., Duan, X., & Chang, L. (2024). Degradation mechanism of methylene blue by heterogenous electro-Fenton with CeO_2/rGO composite cathode. *Colloids and Surfaces A*: *Physicochemical and Engineering Aspects*, *690*, Article 133861. https://doi.org/10.1016/j.colsurfa.2024.133861

Tan, Y., Zhao, C., Chen, Q., Li, L., Wang, X., Guo, B., Zhang, B., & Wang, X. (2023). Heterogeneous electro-Fenton-catalyzed degradation of rhodamine B by nano-calcined pyrite. *International Journal of Environmental Research and Public Health*, *20*(6), Article 4883. https://doi.org/10.3390/ijerph20064883

Tesnim, D., Díez, A. M., Amor, H. B., Sanromán, M. A., & Pazos, M. (2024a). Synthesis and characterization of eco-friendly cathodic electrodes incorporating nano Zero-Valent iron (NZVI) for the electro-Fenton treatment of pharmaceutical wastewater. *Chemical Engineering Journal*, *502*, Article 158099. https://doi.org/10.1016/j.cej.2024.158099

Tesnim, D., Diez, A. M., Hedi, B. A., Sanroman, M. Á., & Pazos, M. (2024b). Sustainable removal of antipyrine from wastewater via an Eco-Friendly heterogeneous Electro-Fenton-like process employing Zero-Valent iron nanoparticles loaded activated carbon. *Chemical Engineering Journal*, *493*, Article 152494. https://doi.org/10.1016/j.cej.2024.152494

Thomas, N., Dionysiou, D. D., & Pillai, S. C. (2021). Heterogeneous Fenton catalysts: A review of recent advances. *Journal of Hazardous Materials*, *404*, Article 124082. https://doi.org/10.1016/j.jhazmat.2020.124082

Thorat, B. N., & Sonwani, R. K. (2022). Current technologies and future perspectives for the treatment of complex petroleum refinery wastewater: A review. *Bioresource Technology*, *355*, Article 127263.

Vialich, J. A., Sugai, D. Y., Wypych, F., Benincá, C., & Zanoelo, E. F. (2022). Electromigration of protons and zero valent iron oxidation: A physico-chemical insight to model the kinetics of Fenton-like process. *Chemical Engineering Journal*, *435*, Article 135026. https://doi.org/10.1016/j.cej.2022.135026

Wang, N., Zheng, T., Zhang, G., & Wang, P. (2016). A review on Fenton-like processes for organic wastewater treatment. *Journal of Environmental Chemical Engineering*, *4*(1), 762–787. https://doi.org/10.1016/j.jece.2015.12.016

Wang, X., Zhu, K., Ma, X., Sun, Z., & Hu, X. (2018). Degradation of diuron by heterogeneous electro-Fenton using modified magnetic activated carbon as the catalyst. *RSC Advances*, *8*(36), 19971–19978. https://doi.org/10.1039/C8RA02776E

Xiao, J., Yue, Q., Gao, B., Sun, Y., Kong, J., Gao, Y., Li, Q., & Wang, Y. (2014). Performance of activated carbon/nanoscale zero-valent iron for removal of trihalomethanes (THMs) at infinitesimal concentration in drinking water. *Chemical Engineering Journal*, *253*, 63–72. https://doi.org/10.1016/j.cej.2014.05.030

Xu, L., & Wang, J. (2012). Magnetic nanoscaled Fe_3O_4/CeO_2 composite as an efficient Fenton-like heterogeneous catalyst for degradation of 4-chlorophenol. *Environmental Science & Technology*, *46*(18), 10145–10153. https://doi.org/10.1021/es300303f

Xu, S., Yang, Y., & Li, F. (2024). Heterogeneous electro-Fenton removal of polyacrylamide in aqueous solution over $CoFe_2O_4$ catalyst. *Water Science & Technology*, *89*(12), 3309–3324. https://doi.org/10.2166/wst.2024.180

Yang, Y., Liu, Y., Fang, X., Miao, W., Chen, X., Sun, J., Ni, B.-J., & Mao, S. (2020). Heterogeneous Electro-Fenton catalysis with HKUST-1-derived Cu@C decorated in 3D graphene network. *Chemosphere*, *243*, Article 125423. https://doi.org/10.1016/j.chemosphere.2019.125423

Yazdanbakhsh, A., Hashempour, Y., & Ghaderpouri, M. (2018). Performance of granular activated carbon/nanoscale zero-valent iron for removal of humic substances from aqueous solution based on Experimental Design and Response Surface Modeling. *Global Nest Journal*, *20*(1), 57–68. https://doi.org/10.30955/gnj.002264

Ye, M., Zhang, C., Liu, Z., Li, H., Fu, Z., Zhang, H., Wang, G., & Zhang, Y. (2023). E-waste derived CuAu bimetallic catalysts supported on carbon cloth enabling effective degradation of bisphenol A via an electro-Fenton process. *Separation and Purification Technology*, *305*, Article 122507. https://doi.org/10.1016/j.seppur.2022.122507

Ye, Z., Padilla, J. A., Xuriguera, E., Beltran, J. L., Alcaide, F., Brillas, E., & Sirés, I. (2020). A highly stable metal–organic framework-engineered FeS_2/C nanocatalyst for heterogeneous electro-Fenton treatment: Validation in wastewater at mild pH. *Environmental Science & Technology*, *54*(7), 4664–4674. https://doi.org/10.1021/acs.est.9b07604

Zárate-Guzmán, A. I., González-Gutiérrez, L. V., Godínez, L. A., Medel-Reyes, A., Carrasco-Marín, F., & Romero-Cano, L. A. (2019). Towards understanding of heterogeneous Fenton reaction using carbon-Fe catalysts coupled to in-situ H_2O_2 electro-generation as clean technology for wastewater treatment. *Chemosphere*, *224*, 698–706. https://doi.org/10.1016/j.chemosphere.2019.02.101

Zare, M. R., Gomnam, F., Darvishmotevalli, M., Mengelizadeh, N., Rahimi, S., Moradalizadeh, S., & Rahmani, A. (2024). Effective degradation of ciprofloxacin from aqueous solutions using heterogeneous electro-Fenton coupled with Fe@ Fe_2O_3 core-shell nanoparticle. *Desalination and Water Treatment*, *320*, Article 100833. https://doi.org/10.1016/j.dwt.2024.100833

Zhang, C., Li, F., Wen, R., Zhang, H., Elumalai, P., Zheng, Q., Chen, H., Yang, Y., Huang, M., & Ying, G. (2020). Heterogeneous electro–Fenton using three–dimension NZVI–BC electrodes for

degradation of neonicotinoid wastewater. *Water Research*, *182*, Article 115975. https://doi.org/10.1016/j.watres.2020.115975

Zhang, J., Qiu, S., Feng, H., Hu, T., Wu, Y., Luo, T., Tang, W., & Wang, D. (2022). Efficient degradation of tetracycline using core–shell $Fe@ Fe_2O_3$-CeO_2 composite as novel heterogeneous electro-Fenton catalyst. *Chemical Engineering Journal*, *428*, Article 131403. https://doi.org/10.1016/j.cej.2021.131403

Zhu, Y., Zhu, R., Xi, Y., Zhu, J., Zhu, G., & He, H. (2019). Strategies for enhancing the heterogeneous Fenton catalytic reactivity: A review. *Applied Catalysis B*: *Environmental*, *255*, Article 117739. https://doi.org/10.1016/j.apcatb.2019.05.041